Journal of Structural Geology, Vol. 13, No. 5, pp. 517 to 537, 1991
Printed in Great Britain

0191-8141/91 $03.00 + 0.00
Pergamon Press plc

Modes of extension at oceanic spreading centers: evidence from the Solea graben, Troodos ophiolite, Cyprus

ROBERT J. VARGA

Unocal Science and Technology Division, Box 76, Brea, CA 92621, U.S.A.

(*Received* 14 *February* 1990; *accepted in revised form* 10 *December* 1990)

Abstract—The Solea graben in the Troodos ophiolite, Cyprus, represents a preserved Cretaceous-age axial valley formed during a brief period of amagmatic seafloor spreading. Structural analysis of all crustal levels of the graben reveals two periods of deformation; an extensive early phase of extensional deformation associated with seafloor spreading and a later phase of minor deformation associated with obduction and doming of the complex during the Tertiary–Recent. Amagmatic extensional deformation produced networks of normal faults that dip toward the graben axis and sole into a regional detachment fault located at the sheeted dike–plutonic contact and oriented subparallel to ophiolite pseudostratigraphy. Individual fault segments are essentially planar but link to approximate listric geometries locally. Bulk structural rotation of fault blocks bounding the graben occurred about a NNW-trending axis, parallel to the present graben trend. Average dips in the sheeted complex within the central portions of the graben suggest 40–50° of structural rotation, although this is a minimum figure because present dike dips are not a simple function of rotation magnitude. Tensor analysis of fault populations associated with extensional deformation shows that σ_3 was oriented approximately perpendicular to the graben axis. Late, near-axis extensional deformation segmented the detachment fault along NNW-trending normal faults. Obduction-related uplift and doming of the Troodos ophiolite is expressed in the Solea graben by minor thrust, reverse and strike-slip faults principally developed during reactivation of pre-existing low-angle fault zones formed during seafloor deformation. Tensor analysis of this later phase of faulting shows that σ_1 was oriented approximately N–S and that σ_2 and σ_3 alternated position during the deformation.

The style of deformation documented in the Solea graben supports recent speculation for Basin and Range-style detachment faulting at slow-spreading ridge crests with low magma budgets, such as parts of the Mid-Atlantic Ridge near large-offset transform faults. Natural cross-sectional exposure of the Solea graben shows how extensional structures might link at depth beneath such slow-spreading ridge segments and demonstrates the importance of extensive brittle deformation of the crust prior to establishment of large-scale (ore-forming) hydrothermal circulation cells.

INTRODUCTION

MODELS for the extensional style of mid-ocean ridge crests (Harrison & Stieltjes 1977, Macdonald & Atwater 1978, Macdonald 1982, 1986) are largely derived from three-dimensional inferences made from two-dimensional images (Vogt & Tucholke 1986) of structures on the seafloor. The inferred geometry of these structures in the third dimension is constrained only through very limited deep drilling (Anderson *et al.* 1982, Leg 118 Shipboard Scientific Party 1988), geophysics (White 1984, McClain *et al.* 1985, Mutter *et al.* 1985), modelling (Tapponnier & Francheteau 1978, Sleep & Rosendahl 1979), and seabed observations and shallow drilling in highly denuded areas near transform boundaries (Leg 109 Shipboard Scientific Party 1986, Karson *et al.* 1987, Karson & Winters 1987). Although much has been learned about the structure of ridge crests from these studies (i.e. Macdonald 1982), many important questions remain unresolved or controversial, such as the possible existence and importance of low-angle normal faults, the temporal interplay between structural and magmatic extensional processes, and the role of structural development in establishment of large-scale black smoker hydrothermal systems.

Ophiolites, subaerial exposures of oceanic lithosphere, potentially can provide details of the nature of extensional processes operating in various oceanic spreading regimes at crustal and upper mantle depths which are otherwise unresolvable in the modern oceans. Several factors have, however, made direct comparison of the structure of ophiolites and modern ocean crust difficult. By the nature of their emplacement through obduction processes (Moores 1982), many ophiolites are fragmented and have polyphase structural fabrics, with late obduction-related structures largely obliterating early seafloor structures. Also, the tectonic environment of formation of some ophiolites is unknown because their geochemistry is unlike that of rocks encountered in typical mid-ocean environments (Miyashiro 1973, Pearce & Cann 1973). Finally, because evidence for preserved spreading centers is rare, the position of most exposed ophiolites within their pre-obduction spreading framework is generally unknown. Thus, even if early seafloor structures can be discerned, it is difficult to determine which structures formed at, or near, a ridge crest and which formed significantly off axis. For these reasons, ophiolites have largely been ignored in formulating models for ridge crest extension processes, particularly for brittle extension within the upper crust.

The Tethyan Troodos ophiolite in Cyprus and Semail ophiolite in Oman offer some of the best exposures in which to observe relatively intact upper crustal oceanic structures which are little affected by obduction and post-obduction disturbances. In contrast to the Semail ophiolite which is elongate in exposure primarily *parallel*

to paleo-spreading direction (Pallister 1981, Nicolas *et al.* 1988), the Troodos ophiolite (Fig. 1) is elongate in exposure *perpendicular* to paleo-spreading direction and is, thus, well-situated for study of oceanic structures in the extension directon. An additional unique feature of the Troodos ophiolite is preservation of an oceanic graben, the Solea graben (Figs. 1 and 2), believed to be a fossil axial valley of a Cretaceous-age spreading center (Varga & Moores 1985, in press). The crustal section of the Solea graben is exposed in oblique cross-section, from sediments, volcanics and large black smoker-type ore bodies in the upper parts of the graben, to its roots in paleo-mantle exposures of Mt Olympos (Fig. 1). The structures found within these exceptional exposures provide insights into the deeper structure beneath active oceanic spreading centers.

Previous reports on the geology of the Solea graben region have outlined the tectonic and geochemical evolution of the area and have emphasized correlations with structural and hydrothermal processes occurring within modern oceanic ridge systems (Varga & Moores 1985, 1986, in press, Allerton & Vine 1987, Hurst *et al.* 1987, Schiffman *et al.* 1987, in press, Schiffman & Smith 1988, Bettison-Varga & Varga 1989, Moores *et al.* in press). The primary purpose of this paper is to present details of the internal structure of the Solea graben to better document the styles of extension active during seafloor spreading. The general geometry of the effects of extensional deformation on vertical markers (sheeted dikes within the upper crust) is developed and is documented through several outcrop-scale deformed zones in the graben. The scale and extent of probable obduction-related deformation of the graben is also discussed.

The non-MORB character of igneous rocks from the Troodos ophiolite has long been known (e.g. Miyashiro 1973, Rautenschlein *et al.* 1985) and has led to a number of models invoking formation of the ophiolite within a suprasubduction setting (see Moores *et al.* 1984). Despite these suggestions, the Troodos ophiolite, and more specifically the Solea graben, display a number of structural characteristics which are compatible with many seafloor and drill hole observations of crust formed at mid-ocean spreading centers. Because the style of upper crust extension may be similar in a variety of oceanic settings, as it appears to be in various continental extensional environments, the *processes* of spreading in the Solea graben are emphasized in this paper. Thus, the modes of extension documented here may find applicability in a number of oceanic spreading environments, in mid-ocean, or in arc-related settings.

STRUCTURAL GEOLOGY

General relationships

The regional structural geology of the Troodos ophiolite is shown in Fig. 1. In this figure, the sheeted dike complex is divided into a number of orientation domains in which dikes either have similar dip azimuths or dip toward each other in a complementary fashion. The significance and paleomagnetism of these domains is discussed in Moores *et al.* (in press). The Solea and Mitsero domains have been shown to represent structural grabens through mapping (Varga & Moores 1985, Ramsden 1987) and geophysical methods (Hurst *et al.* 1987, G. Constantinou personal communication 1987). Relatively large Cu–Zn massive sulfide bodies (Constantinou & Grovett 1973) of black smoker-type preferentially occur within the volcanic sections of the Solea and Mitsero grabens. Varga & Moores (1985) suggested that Solea, Mitsero and Larnaca grabens are fossil axial valleys, formed and preserved through successive eastward jumps of a Cretaceous-age spreading center. Subsequent work on the boundary between the Solea and Mitsero grabens (Hurst *et al.* 1987) supports the inference that the Solea graben is indeed older and that its much narrower eastern flank (Fig. 1) may be due to

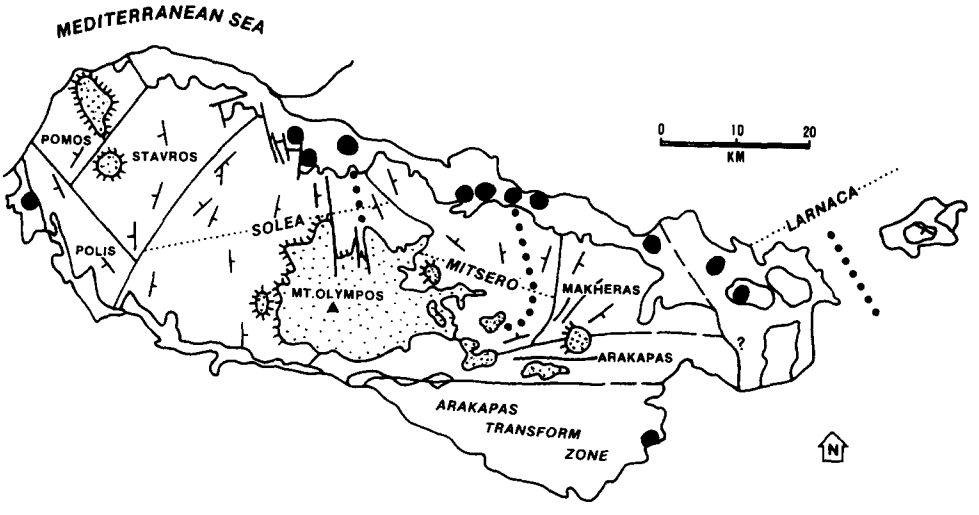

Fig. 1. Generalized map of the Troodos ophiolite showing orientation domains within the sheeted dike complex. Average dike orientations are shown by the strike and dip symbols. Stippled areas are main exposures of gabbro and ultramafic rock. Hachured contacts between sheeted dike complex and stippled region represent elements of extensional detachment zone. Blackened areas are large ($>0.5 \times 10^6$ tons) massive sulfide ore bodies within the volcanic section of the ophiolite. After Moores *et al.* (in press).

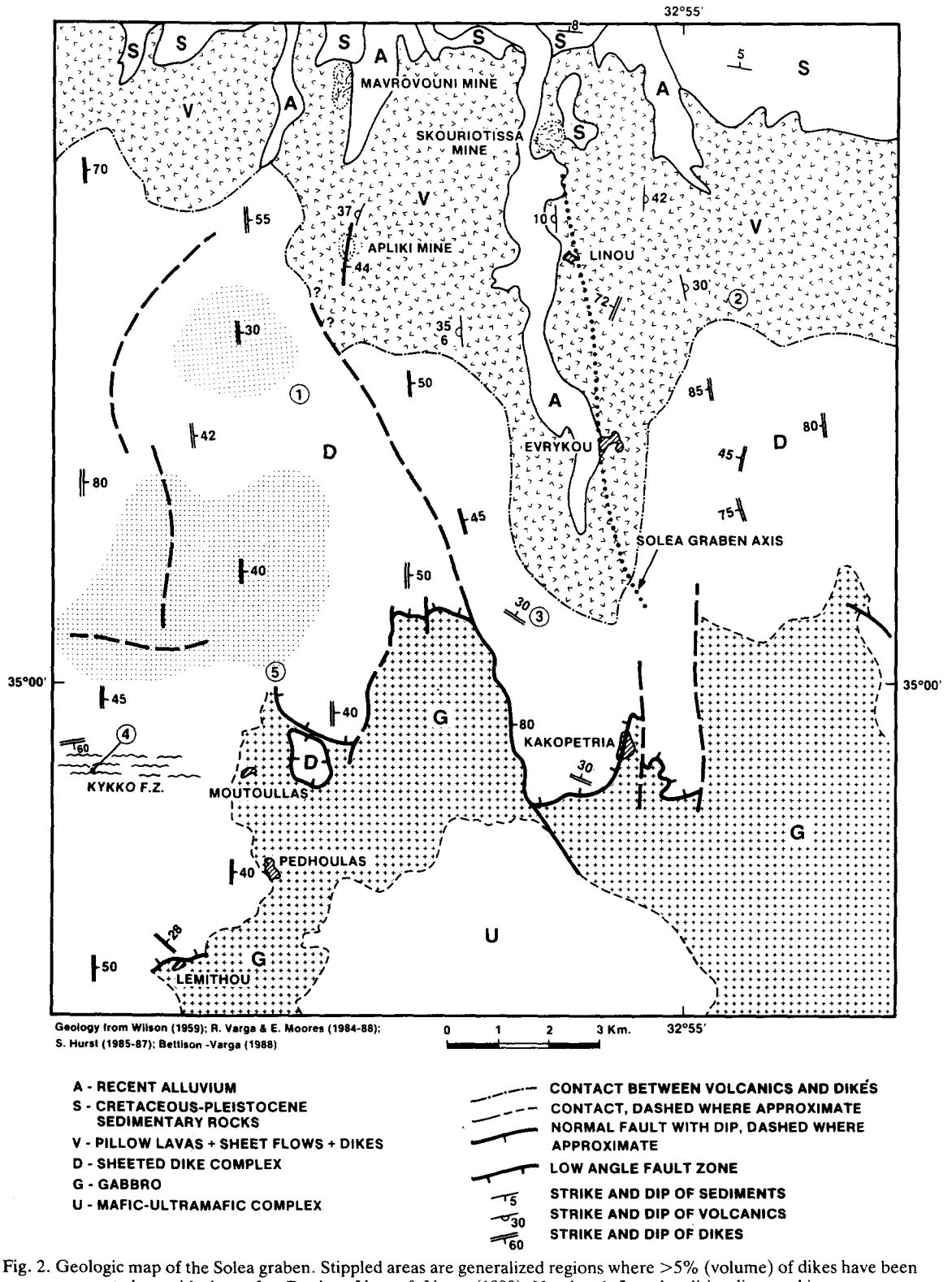

Fig. 2. Geologic map of the Solea graben. Stippled areas are generalized regions where >5% (volume) of dikes have been converted to epidosites, after Bettison-Varga & Varga (1989). Number 1–5 are localities discussed in text.

eastward ridge migration. As discussed by Allerton & Vine (1987) and Moores *et al.* (in press), however, other plate geometries are possible. In particular, Allerton & Vine (1987) suggest that the geometric asymmetry of the Solea graben may be due to an extension geometry similar to the uniform-sense, simple shear model invoked by Wernicke (1985) for continental extension.

Doming and unroofing of the Troodos ophiolite has exposed the plutonic and mantle foundation of the Solea graben on Mt Olympos (Figs. 1 and 2). At least part of this uplift represents a preserved mantle diapir (Nicolas *et al.* 1988) which formed beneath the graben at an oceanic spreading center as discussed in Varga & Moores (in press). This uplift has resulted in the present oblique cross-sectional exposure of the graben. One result of this geometry is exposure of a low-angle normal fault, the Kakopetria detachment, separating highly deformed sheeted dikes from the plutonic section of the ophiolite (Figs. 1 and 2). This zone of complex deformation is believed to have been active during seafloor

spreading and to have functioned as a detachment during a brief period of amagmatic extension at a ridge crest (Varga & Moores 1985, 1986, in press, Bettison-Varga & Varga 1989).

Geometry of extension of upper oceanic crust

Before discussing specific examples of extensional structures within the Solea graben, it is useful to examine the general geometrical aspects of normal faulting upon the upper oceanic crust. This ~2 km-thick layer within ophiolites comprises dominantly thin (~0.5 km) volcanics overlying sheeted diabase dikes and corresponds in a general way to geophysically defined oceanic layer 2 (Moores & Jackson 1974, Fox *et al.* 1980, Karson 1982). It is within this crustal layer that most of the extensional deformation within exposures of the Solea graben is restricted.

An extensive body of literature has developed in the past 10–15 years which discusses the geometric effects of extensional faulting upon sedimentary rocks, where original marker horizons, such as bedding, are originally horizontal prior to faulting (see Wernicke & Burchfiel 1982). The general result of such faulting in areas of significant crustal extension is to steepen sedimentary layering, regardless of whether fault geometries are purely listric, rotational-planar (domino-style of Axen 1988), or some combination of these two end-members. Figure 3(a) illustrates the simple case of sedimentary units disrupted in the hanging wall of a listric-normal fault. Bedding steepens to satisfy the general constraint that the angle (α) between layering and the fault remains constant during extension. In addition to bed steepening, the hanging wall must deform internally as bed length necessarily increases to accommodate rollover and to maintain cross-sectional area. Hanging wall deformation is achieved through a variety of mechanisms, including bed thinning, layer-parallel shear and antithetic faulting (Gibbs 1983, 1984, Williams & Vann 1987). A single antithetic fault, making an original angle of ϕ to bedding, is shown in Fig. 3(a). With increased horizontal extension, the antithetic fault is also rotated such that its observable apparent sense of offset is switched from normal to reverse (Fig. 3a, lower frame).

Some differences arise when applying models of normal faulting derived from studies of continental extension to extension of oceanic crust, aspects of which have been discussed previously (Verosub & Moores 1981, Harper 1982, Varga & Moores 1985, Karson 1987). Figure 3(b) shows a simple listric fault model for exten-

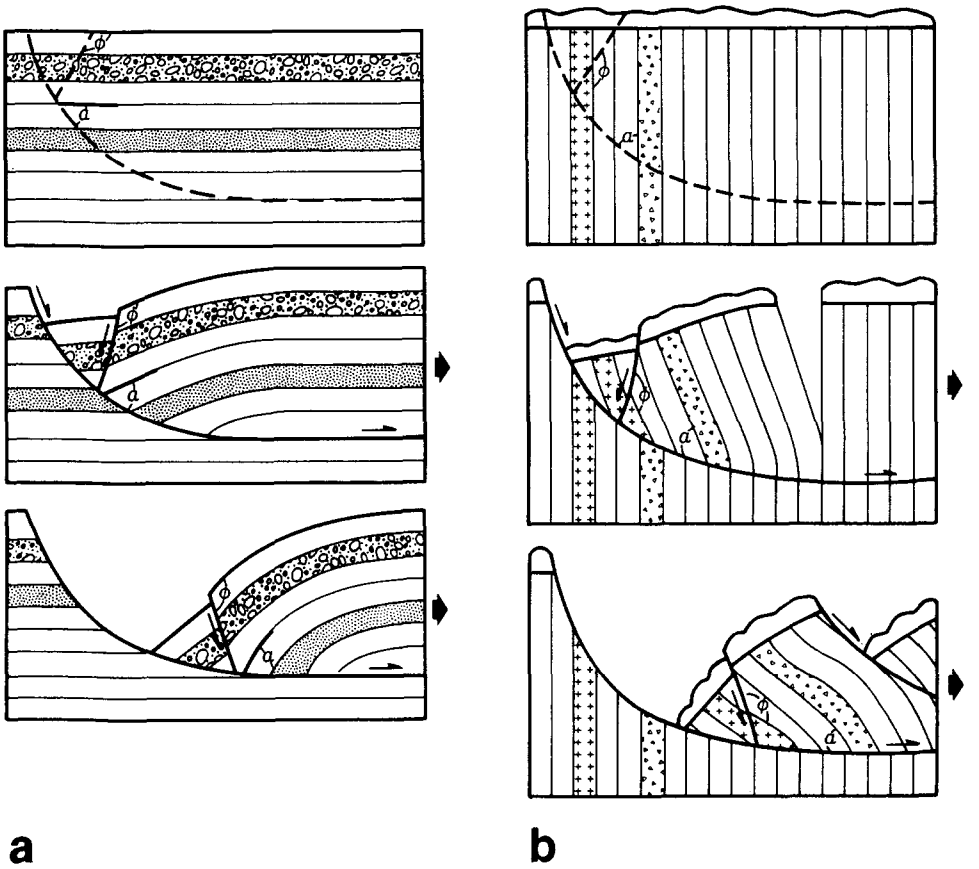

Fig. 3. Simple models for hanging wall rotations above listric normal faults. (a) Case where hanging wall contains horizontal anisotropy (bedding). As extension proceeds, bedding keeps a constant angle (α) with respect to fault surface causing rollover of hanging wall and steepening of bed dips. Requisite bed lengthening of hanging wall can be accommodated through layer-parallel shear or through antithetic faulting. Antithetic fault retains constant angle (ϕ) with respect to layering during extension causing offset-sense reversal to apparent reverse motion. (b) Situation where hanging wall contains primarily steep, near-vertical anisotropy (sheeted dikes). Extension and rotation causes lowering of dike dips and steepening of thin, overlying volcanic section; note that these dip in opposite directions. Lack of original horizontal anisotropy prohibits requisite hanging wall lengthening by subhorizontal shearing. Antithetic faulting is likely mechanism for rollover accommodation.

sion of upper oceanic crust. The geometry of deformation of the originally horizontal volcanic section is basically identical to the sedimentary model (Fig. 3a), in that layering steepens and dips antithetically with respect to the listric fault. In contrast, dikes within the underlying diabase complex are rotated to less-steep orientations from assumed originally vertical dips. Note that the hanging wall of the oceanic model must also deform (thin) due to the constraint of the listric fault geometry. It is important to note that the lack of gently dipping anisotropy within the dike section probably prevents significant hanging wall thinning through mechanisms other than antithetic faulting. Thus, the hallmark of extended mid- to upper-crustal oceanic sections should be volcanics which dip in the opposite direction from master normal faults and dikes. Also, antithetic normal faults, potentially rotated to reverse apparent separations, might be expected in more highly extended regions.

A problem encountered in structural studies of ophiolites is the lack of an originally horizontal reference frame in the rocks below the volcanic section. A tacit assumption in Fig. 3(b) is that dikes of the sheeted diabase complex are originally emplaced vertically beneath more-or-less horizontal volcanics. Accepting this assumption, which is discussed more fully below, one can solve for the mutual geometry of dike–volcanic pairs undergoing extension. For this exercise, we can assume that the rotational axis is approximately horizontal, as is generally the case in extensional environments. With this constraint, rotation of originally horizontal volcanics on listric or rotational-planar normal faults will result, stereographically, in a great-circle distribution of bedding poles about the rotational axis; bed dip is a direct measure of the amount of bed rotation. In contrast, the dip of deformed dikes is not a simple function of rotation amount as assumed in the simple model presented by Norrell & Harper (1988). The final dip of originally vertical dikes is quite sensitive to the original angle between the dike and the rotational axis. In the most simple case for a horizontal axis of rotation, the *minimum* attainable dike dip is increased as the angle between the dike and fault increases (Fig. 4a); the final dip of rotated dikes cannot be less than the magnitude of the angle between the trend of the rotation axis and the original dike strike. For example, if the dike strike makes an original angle of 30° with the trend of the horizontal rotational axis, the dike cannot attain a dip of less than 30°, even after 90° of body rotation (Fig. 4a). Thus, *dips of individual dikes are only indicators of the minimum amount of structural rotation*. Another effect of rotation of originally vertical dikes is strike dispersion for dikes not originally parallel to the rotational axis. This dispersion is depicted in Fig. 4(b). As extension proceeds, the angle between the final dike strike and the rotational axis will increase dramatically, approaching 90° except for those dikes with original strikes parallel to the rotational axis (Fig. 4b).

Figures 4(a) & (b) predict that in most natural examples, originally vertical markers, such as sheeted

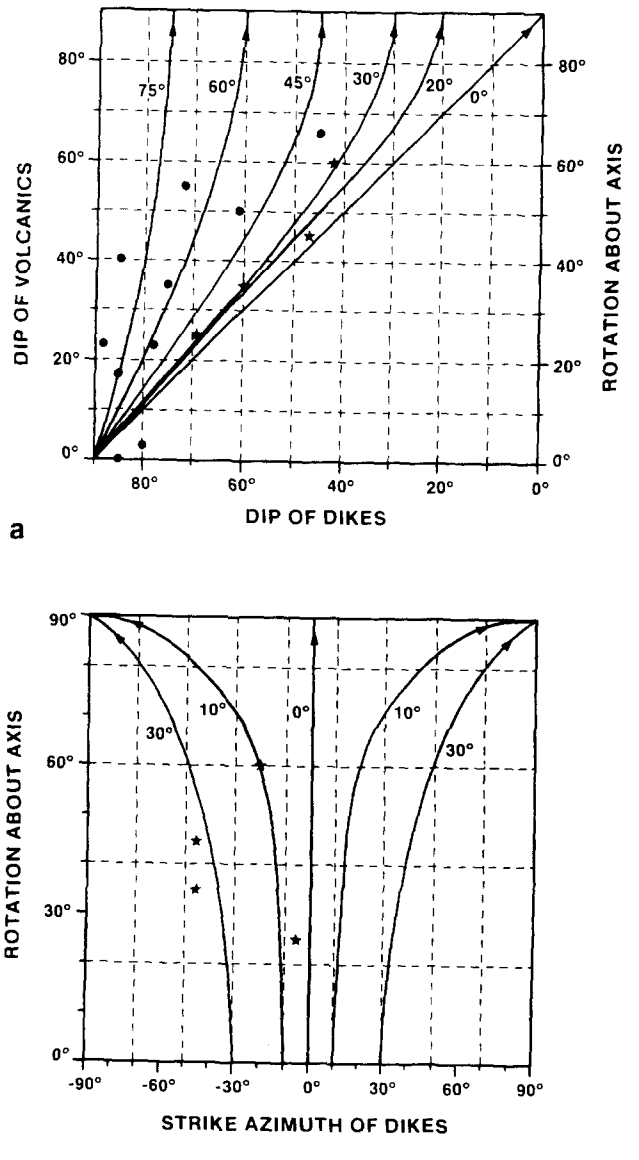

Fig. 4. (a) Graph showing change in dip of originally vertical dikes vs amount of structural rotation about a horizontal axis. Trajectories (curves with arrows) show rotation paths for dikes making various original angles (shown next to trajectories) with respect to rotational axis. For dike–volcanic pairs, dip of volcanics is a direct measure of rotation magnitude. Plotted data are for dike–volcanic pairs measured in the Solea graben region. Points plotted as stars lie within ~30° of the rotational axis. (b) Graph showing change in strike azimuth of originally vertical dikes vs amount of structural rotation. Trajectories (curves with arrows) show rotation paths for dikes making various original angles (shown next to trajectories) with respect to rotational axis. Data plotted are from dike–volcanic pairs where pre-rotational dike strike was determined to lie within about 30° of rotational axis (star symbols in a).

dikes will show much more variation in strike orientation after rotation during extension than originally horizontal markers. Plotted stereographically, poles to individual dikes will follow small-circle paths about the rotational axis while poles to originally horizontal volcanic bedding will plot along a great-circle. For a population of dikes with original strikes that fluctuate 30–40° about the rotational axis, extension will result in dike poles that plot within a very dispersed zone; the axis of this zone will be the rotational axis. Figures 4(a) & (b) also predict that, for a given amount of rotation, the strike of dikes with the lowest dips will tend to more

closely approximate the true rotational axis than any other. Also, some estimate of the orientation of the rotational axis can be derived by plotting data from measured dike–volcanic pairs on a diagram similar to Fig. 4(a). Strike directions of dikes from dike–volcanic pairs plotting along rotational trajectories less than about 30° in Fig. 4(a) should lie the closest to the axis of rotation. It should be emphasized that Figs. 4(a) & (b) do not take into account local variations in the orientation of the rotational axis due to variations in fault orientation and kinematics. Additionally, analysis of the rotational parameters of the upper crustal section of ophiolites and oceanic crust can locally be complicated by presence of significant (>20°), pre-faulting, constructional dips within volcanics (e.g. Ballard & Van Andel 1977). Such variations will undoubtedly result in much more data scatter.

Limited direct observation of dikes and associated lavas near oceanic spreading centers (see Karson 1987) supports the hypothesis that dikes in the sheeted complex are generally emplaced vertically. Dike strike can be inferred from tension fracture and fault orientations (Karson 1987) near spreading centers to be more-or-less parallel to the regional trend of the ridge axis. In detail, dike strikes, as inferred from observed surface fissures, potentially can deviate significantly from the orientation of the local spreading axis, especially at slow-spreading ridges and near transform boundaries (Karson & Dick 1983, Gallo *et al.* 1984, Karson *et al.* 1984). Extensional deformation of dikes with such variation in initial orientation will result in complex rotations as described above.

Extensional structures above the Kakopetria detachment

The Solea graben (Fig. 1) is defined by the 'V-shaped' pattern of the sheeted dike–volcanic contact which is a result of the gentle (~10° to the north) dip of lithologic units in the region. The graben is approximately 10–12 km in maximum width and has 2–3 km of structural depth. In general, volcanic layers dip away from the NNW-trending graben axis while dikes and normal faults show the complementary relationship (Figs. 2 and 5a). Although relatively rare, several good outcrops were found where the dikes cut pillow lavas and sheet flows (Fig. 5b) and where the angle between the two could be measured. Figure 7 shows a graph of the angle between dikes and associated lavas plotted against dike dip. These data show that the angle between dikes and volcanics is generally high (average ~78°) and can be considered essentially an orthogonal relationship. This nearly orthogonal relationship indicates that, where measured, original constructional dips within the volcanics were low. Figure 7 also indicates that the angle between dikes and volcanics is not a function of dike dip, suggesting that non-vertical dike dips are the result of tectonic rotation following injection and that little or no tectonic shear strain has occurred within the section. Post-injection, tectonic rotation of non-vertical dikes has been confirmed by paleomagnetic results at several sites in the sheeted complex of the graben (Allerton & Vine 1987, Hurst *et al.* 1987, Moores *et al.* in press).

Figure 8 is a sketch of typical dike–fault relationships found along the west side of the graben which illustrates well the geometry of extensional faults above the Kakopetria detachment fault. Dikes in this area (locality 1, Fig. 2) are rotated to moderate to low dips along a series of interconnecting, planar-normal faults. In general, dikes dip either less steeply or are parallel to the faults which truncate them at depth. Individual faults show some concave-upward (listric) curvature, but this is not common and faults are best described as essentially planar. As shown on Fig. 8, planar fault segments connect to approximate listric geometries overall. A consistent relationship of high-angle normal faults cutting low-angle faults (Jackson & McKenzie 1983, Miller *et al.* 1983) was not observed, although this is the case at a much larger scale as discussed below. Structural data from the outcrop shown on Fig. 8 is plotted stereographically in Fig. 9(a). Normal faults dip NE or SE at moderate to low angles with highly variable strike and slickenside directions. High-angle transfer faults strike NE but are not visible in Fig. 8 because they are approximately parallel to the outcrop. Transfer faults related to extension typically are bounded above and below by normal faults and serve to compartmentalize fault blocks. Poles to dikes (Fig. 9a) plot primarily SW.

Fault–dike relationships on the east side of the graben are similar to, but a mirror image of, those on the west. Figure 10 shows a sketch of one eastern outcrop (locality 2, Fig. 2) and structural data from this outcrop are plotted stereographically on Fig. 9(b). Normal faults dip SW and NW and limited slickenside data indicate fault-slip to the WSW. A single measured high-angle transfer fault strikes NE (Fig. 9b). Dike dips, as in most of the eastern part of the graben, are to the west except in the middle part of the outcrop where they dip moderately E. These eastern dips form part of a minor antiform within the dike section. This fold is reflected, stereographically, by the approximate great-circle distribution of poles to dikes (Fig. 9b). The axis of this fold plunges shallowly to the NNW. This and several similar NW-trending fold structures found within the Solea graben are interpreted as due to rotation of dikes through angles greater than 90° by repeated faulting.

Although relatively uncommon, several examples of antithetic normal faults rotated to reverse apparent offset are observed in the Solea graben. Figure 11 is a sketch of one such area on the west side of the graben (locality 3, Fig. 2). At this outcrop, dikes and faults strike NNW and dip E, but the faults show apparent dip-slip reverse offset such that the hanging wall is offset away from the graben axis. These faults are interpreted as rotated antithetic normal faults formed early in the extensional history when dikes had much steeper angles than presently (Fig. 3). This interpretation is based on the strike-parallelism of these faults with normal faults of the graben and their sense of offset; hanging wall motion is away from the graben axis (Fig. 3). Reverse

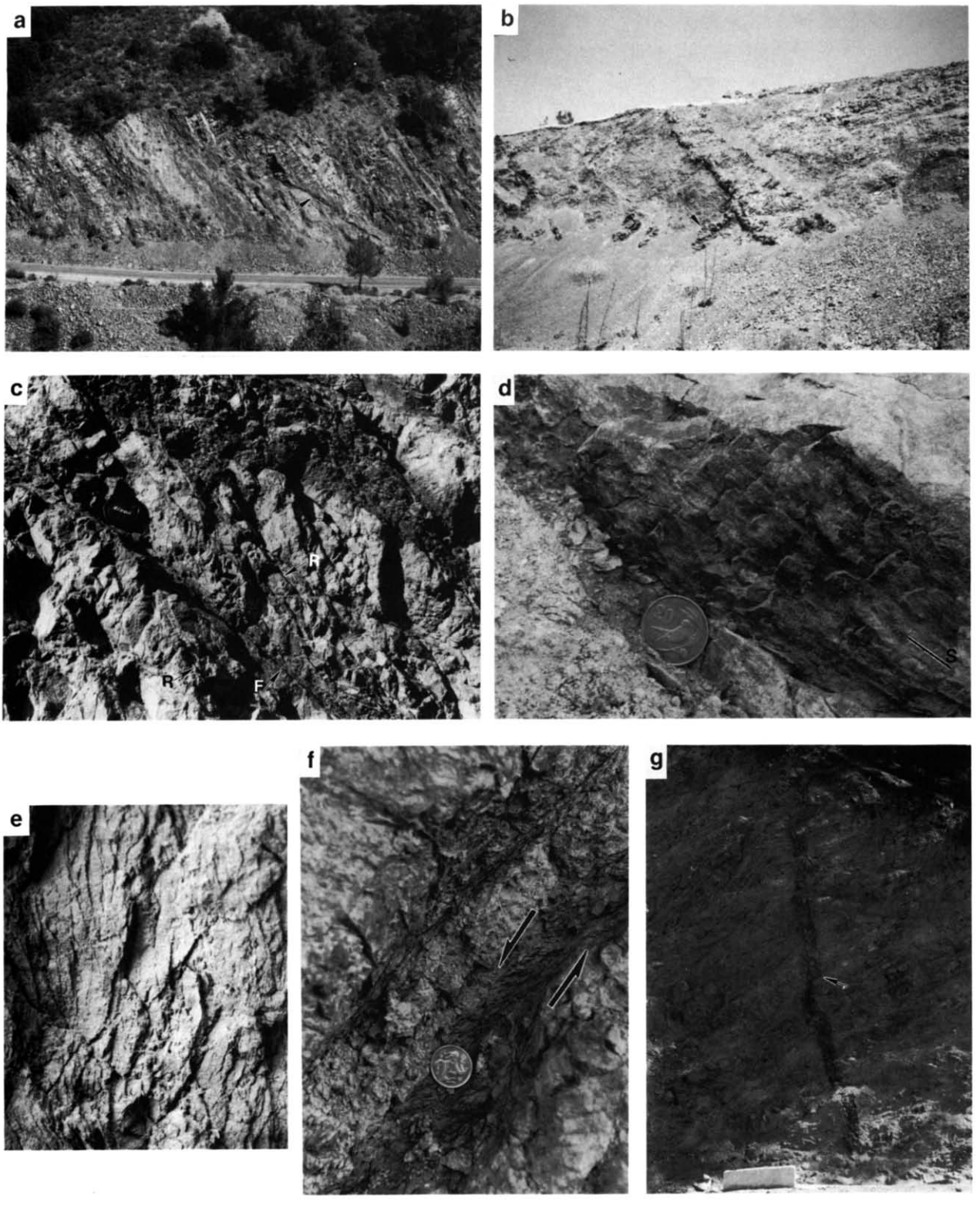

Fig. 5. (a) Photograph (direction of view is to the north) of a low-angle normal fault (arrow) cutting structurally tilted, E-dipping dikes on the west side of the Solea graben. Note that both dikes and fault dip in the same direction. (b) Photograph (direction of view is to the north) of an E-dipping dike on the west side of the Solea graben cutting W-dipping sheet flows (arrow). Note approximate apparent orthogonal relationship between dike and flows. (c) Photograph viewing normal fault and related Riedel structures parallel to strike. Main fault trace (F) dips to the right at about 40°. Higher angle subsidiary faults (R), interpreted as Riedel shears, dip to right and cut both hanging wall and footwall. (d) Photograph of surface of an oblique-slip fault showing RM-type Riedel structures indicating relative sinistral motion. Note steps on fault surface perpendicular to slickenside lineation (S). Coin is approximately 2.7 cm in diameter. (e) Photograph of strike-slip fault surface showing RO-type Riedel structures indicating dextral motion. Outcrop is about 1 m across. (f) Photograph showing foliated fault gouge within fault dipping about 45° to the left. Foliation within gouge dips less steeply to the left indicating normal motion. Coin is approximately 1.9 cm in diameter. (g) Photograph (direction of view is to the east) of numerous N-dipping (to left) minor faults cutting gabbro between Pedhoulas and Moutoullas. Diabase dike cuts faults but is offset by minor thrust reactivation (arrow). Outcrop is approximately 2.5 m across.

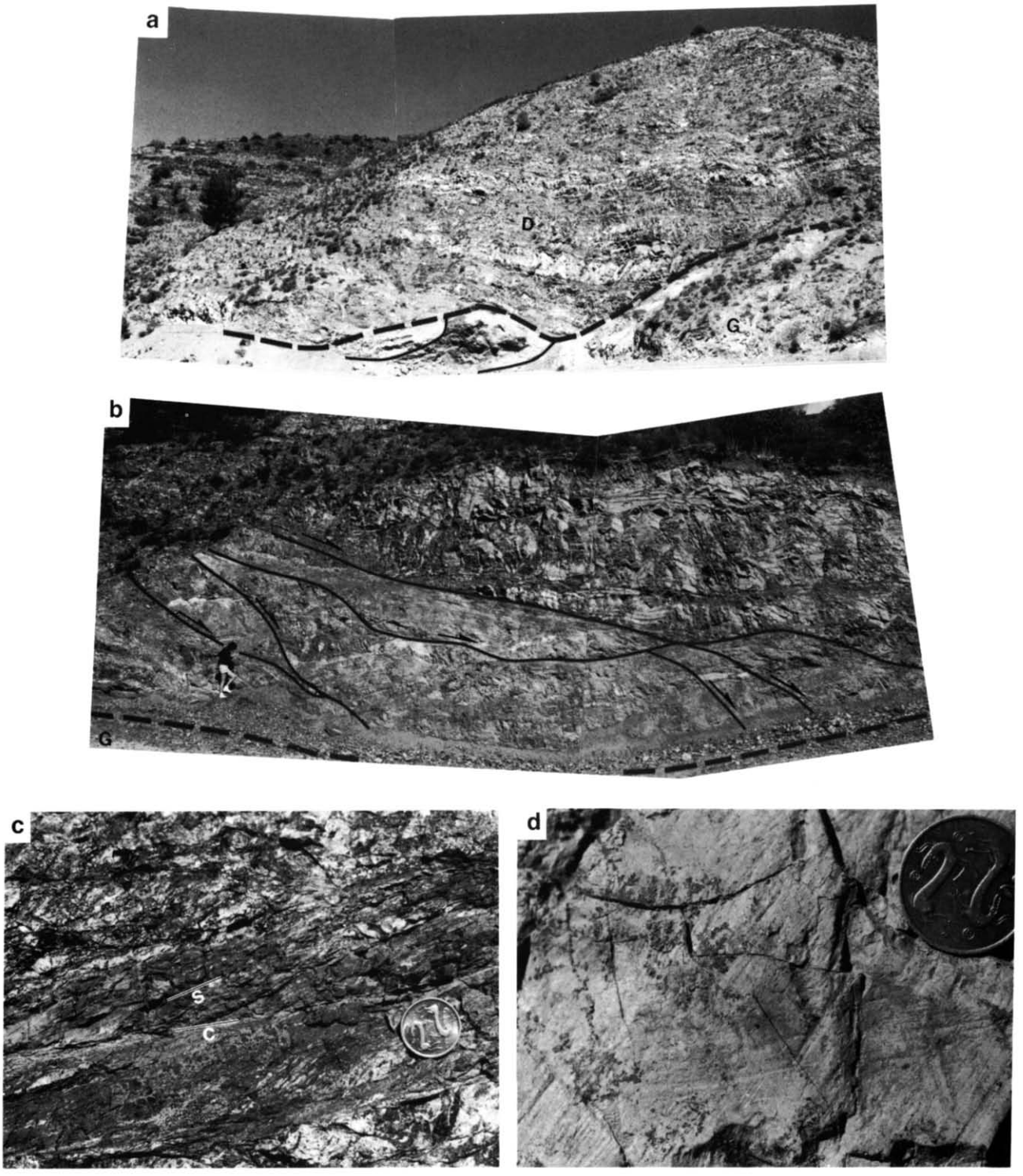

Fig. 6. (a) Photograph montage (direction of view is to the NNW) of the Kakopetria detachment (bold dashed line) at Lemithou separating highly rotated sheeted dikes (D) from sheared gabbro (G). Light lines trace several curved fault surfaces within gabbro defining meter-sized lensoidal blocks. (b) Photograph montage (direction of view is to the north) of deformed sheeted dikes in hanging wall of detachment fault (bold dashed line) at Lemithou. Area shown is approximately 30 m west of area shown in (a). Light lines trace several of the myriad of E-dipping normal faults cutting the dike section and apparently rooting into the detachment. Gabbro (G) is exposed along the road bed beneath the detachment. (c) Photograph looking to the north of early deformation textures within gabbro in the detachment zone at Lemithou. *S–C* relationships here indicate top-to-the-east motion, sympathetic to normal fault motion for hanging wall normal faults in dikes (Fig. 15b). (d) Photograph of high-angle fault surface cutting volcanic rocks near village of Linou (Fig. 2). Fault strikes NNW and dips steeply E. An early phase of oblique-slip normal motion is indicated by slickensides plunging moderately to the left side of photograph. These are partially overprinted by near-horizontal slickensides produced during strike-slip reactivation of the fault. Coin is approximately 1.9 cm in diameter.

and thrust faults related to emplacement (discussed below) generally have more E–W strikes.

Without exception, faults related to extension and graben formation above the Kakopetria detachment are brittle features; no evidence for ductile deformation was observed even at the lowest structural depths of the sheeted complex. Kinematic indicators along the fault surfaces reflect their brittle history. The most common features for indicating fault motion in the area are RM-type (Figs. 5c & d) and RO-type (Fig. 5e) Riedel shear–fault relationships (Petit 1987). Other kinematic indicators include offsets of petrologically distinctive dikes, offset breccia fragments, and obliquely foliated fault gouge (Fig. 5f) (Chester *et al.* 1985).

Figure 12 shows all faults measured within the Solea graben above the Kakopetria detachment, excluding data measured in the area of the Kykko fault zone (Fig. 2, locality 4) and within dikes immediately above the detachment near Lemithou (Fig. 1). Although the diagrams are somewhat difficult to interpret, the general pattern emerges of normal faults on either side of the graben dipping toward the graben axis and probable tear faults trending NE. The diagrams are complicated by inclusion of probable compressional emplacement structures discussed below.

The amount of extension represented by the Solea graben was estimated by Norrell & Harper (1988) to have been approximately 90%. Their estimation was based on a geometric model invoking multistage, domino-style (Nur *et al.* 1986, Axen 1988) faulting and an average of 40° of dike rotation based on the paleomagnetic work of Allerton & Vine (1987). A more conservative estimate of the amount of extension is derived by area-balancing over the total graben width. Assuming an original 3.2 km thickness of the volcanic and sheeted dike section (Moores & Jackson 1974), a 12 km graben width, and the asymmetric cross-sectional profile, results in an estimate of total average tectonic extension across the graben of approximately 45%. The difference between these two results may, in part, be due to the much greater extension estimates resulting from use of a rotational-planar fault model over a listric fault model, an effect noted by Norrell & Harper (1988). However, the difference in extension estimates is probably more a result of considering different scales. Extension varies greatly across the graben and is obviously larger near its axis where structural depth is at a maximum (Fig. 2); most of the paleomagnetic data (Allerton & Vine 1987) used by Norrell & Harper (1988) are from this axial area. Toward the graben margins, dikes are much steeper (Wilson 1959) and extension-related rotation presumably less. Thus, whereas extension may locally reach 90% or higher, as near the graben axis, the extension across the entire Solea graben is closer to half that amount.

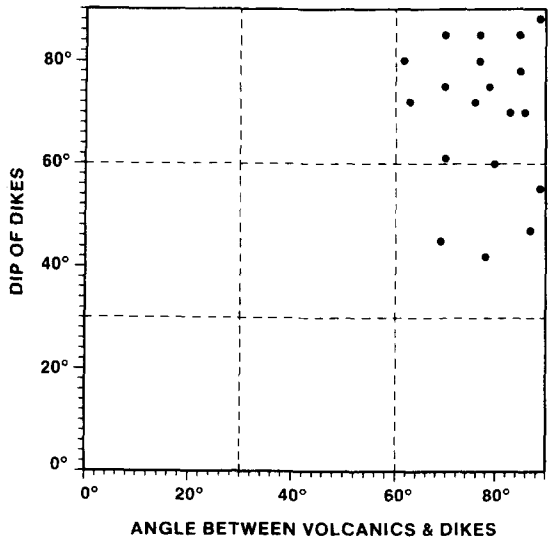

Fig. 7. Graph showing measured angle between sheeted dikes and volcanics in the western Troodos Mountains. Average angle is ~78°. Note that angle does not depend upon the present dip of the dikes supporting the suggestion that they were emplaced approximately vertically.

Rotational axis for extensional deformation

Poles to dikes and volcanic layering measured in the Solea graben are plotted stereographically in Fig. 13. Poles to dikes in the western part of the graben form a diffuse cluster plunging W, whereas poles to volcanics generally plunge moderately E. A similar, but reversed pattern is shown for data from the east side of the graben. Collectively, these data reflect the complementary rotation of dikes and volcanics (Figs. 3b and 5b); clockwise and anticlockwise for the east and west sides of the graben, respectively, as viewed from the south.

Eigenvector analysis (Darot & Bouchez 1976) of dike data from the western side of the graben shown in Fig. 13(a) indicate that the data cluster should be considered statistically homoclinal (mean pole oriented 43°/276°). This is in part due to the wide spread in initial dike strike orientation, as evidenced by the diversity in strikes of steep dikes within the western graben (Fig. 13a). In contrast, data from the east side of the graben (Fig. 13b) statistically lie along a great-circle indicating a rotational axis of 17°/338°. All of the data from the east and west sides of the graben are plotted together in Fig. 13(c). The data lie along a very diffuse, nearly E–W-striking great-circle indicating a best-fit axis of rotation oriented 2°/002°. This result is obviously heavily biased by data from the west side of the graben.

Data for dike–volcanic pairs from individual outcrops are plotted on Fig. 4(a). Using the model discussed above, the scatter in the data reflect the spread in initial dike strike orientations prior to extensional faulting. Four data points, shown by star symbols are those that lie close to the rotational trajectories for original dike strike orientations within ~10–30° of the assumed horizontal rotation axis. These highlighted data are plotted on Fig. 4(b) and indicate that the axis of overall dike rotation is approximately N10°–30°W. A NNW-trending rotational axis is in agreement with the strike of the graben symmetry axis (Fig. 2) and with the interpretation of paleomagnetic data on rotated dikes in the graben by Allerton & Vine (1987). Their analysis led to

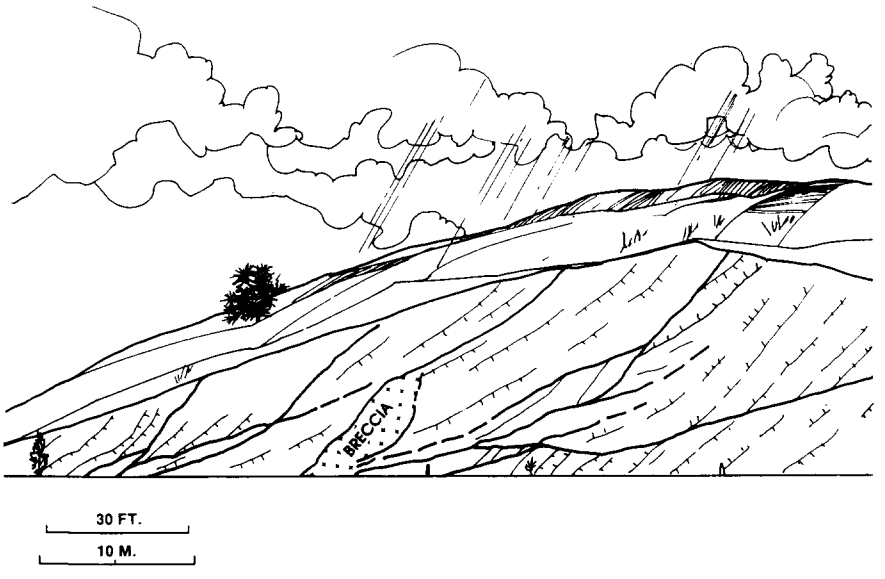

Fig. 8. Outcrop sketch (direction of view is to the south) of roadcut exposures at locality 1 (Fig. 2). Light lines with hachures represent dike margins; heavy lines represent normal faults. Note how faults comprise planar segments that link to form approximately listric geometries.

two non-unique solutions due to the lack of local paleohorizontal control. One solution required structural rotations averaging over 90°, while the geologically most reasonable solution required average structural rotations of less than 90° about NNW-trending rotational axes. Interestingly, this latter solution resulted in restored NNW-trending dike strikes, approximately parallel to the strike of the graben axis.

Timing of extensional deformation

The timing of extensional deformation and formation of the Solea graben has been previously discussed by Varga & Moores (1985, 1986, in press), Schiffman *et al.* (1987), Bettison-Varga & Varga (1989) and Moores *et al.* (in press). Most outcrops do not contain cross-cutting relationships that allow relative dating of local faulting and structural rotations. However, in several areas, steep, non-rotated and undeformed dikes cut highly faulted and rotated dikes. Bettison-Varga & Varga (1989) have also shown that extensional structures controlled the initial fluid flow within the upflow zone of a high-temperature, seawater-dominated, hydrothermal upflow zone (Schiffman *et al.* 1987, in press, Schiffman & Smith 1988) located in the western part of the graben (Fig. 2). The upflow zone is characterized in the field by extensive regions in which the original mineralogy of diabase dikes has been recrystallized to granular mixtures primarily of epidote + quartz ± chlorite termed epidosites. Near the peripheries of the upflow zone, brecciated regions within normal fault zones preferentially contain epidosite-type alteration assemblages (Fig. 14). Further, several normal faults within the zone of epidosite alteration are intruded by late gabbro stocks (Bettison-Varga & Varga 1989). Together, these relationships indicate that extensional deformation and formation of the Solea graben occurred prior to emplacement and at or near an oceanic spreading center.

Kakopetria detachment

Varga & Moores (1985) documented an extensive fault zone separating highly rotated dikes of the Solea graben from underlying gabbro and extending into the upper ~2–100 m of the gabbro. The overall sense of offset across this zone is normal and has been termed the Kakopetria detachment because of its gross similarity to regional normal fault zones observed in the western U.S. Basin and Range (e.g. Wernicke & Burchfiel 1982, Miller *et al.* 1983, Wernicke 1985). The detachment is documented at many locations throughout the Troodos ophiolite (Fig. 1) and is believed to presently be a major groundwater aquifer (Moores *et al.* in press). Because of temporal variations in the amount of tectonic extension during construction of the ophiolite, the detachment is best-developed in areas with the most extreme rotations of sheeted dike, such as in the Solea area and near Pomos (Fig. 1) in the western Troodos Mountains.

In the Solea graben, the Kakopetria detachment is expressed as several E–W-trending, faulted contact segments between the sheeted dikes and gabbros (Fig. 2). The detachment segments generally parallel the ophiolite pseudostratigraphically and dip gently (10–20°) N as a consequence of probable obduction-related doming of the complex. In several areas, the detachment segments are bounded by N- to NW-striking, high-angle normal faults. The best exposed of these high-angle faults runs NW, from approximately 2.5 km west of Kakopetria to 1–2 km west of the Apliki Mine (Fig. 2). Approximately 800 m of normal offset has occurred along this particular fault (S. Hurst personal communication 1988). A fault contact has not been identified between the offset detachment segments at Lemithou and east of Moutoullas. Abundant plagiogranite bodies occur along this zone (S. Hurst personal communication 1988), however, which may have intruded along a pre-existing fault zone between the two segments.

The hydrothermal setting of rocks associated with the

Kakopetria detachment is discussed by Schiffman *et al.* (1987), Schiffman & Smith (1988) and Varga & Moores (in press). Dikes within a few meters of the detachment are epidosites and contain appreciable amounts of base metal sulfides. Gabbro beneath the fault contains prehnite–actinolite facies mineral assemblages and is cut by numerous laumontite veins that do not cross the detachment. The pattern of hydrothermal alteration of these rocks, combined with interpretation of oxygen isotopic data, suggests that the detachment zone acted as the permeable base of a subhorizontal zone of fluids flowing laterally through the faulted sheeted dike section; this zone was characterized by high temperatures and high fluid/rock ratios. In contrast, the detachment was underlain by a hydrothermal zone characterized by high temperatures, but low fluid/rock ratios in the plutonic section.

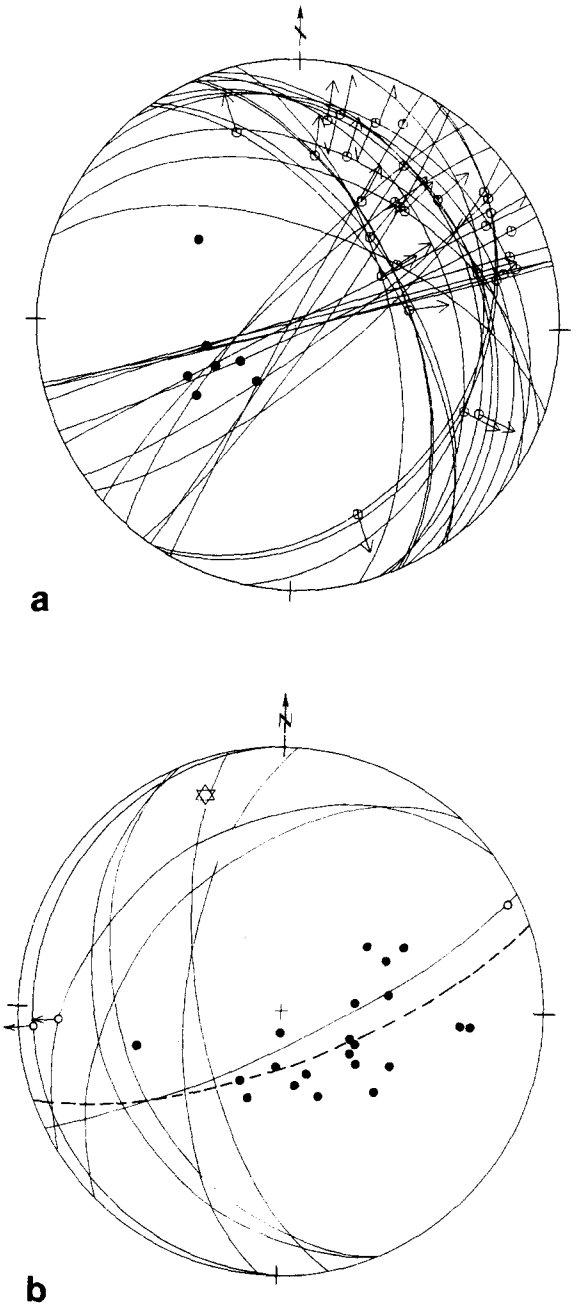

Fig. 9. (a) Equal-area stereonet showing cyclographic traces of faults and poles (dots) to dikes measured at locality 1 (Figs. 2 and 8). Small circles on fault traces indicate slickensides. Full arrows show relative motions of hanging walls with respect to footwalls for faults with relatively high-raking slickensides and half arrows show relative lateral motion on faults with low-raking slickensides. (b) Fault and dike data for locality 2 (Figs. 2 and 10). Symbols as in (a). Star is pole to great-circle (dashed line) through dike poles.

Recent detailed work on the Kakopetria detachment has shown that it is much more structurally complicated than previously thought. While the general geologic relations demonstrate that the fault has normal offset, the zone has a polyphase history with numerous, minor obduction-related faults overprinting, and in part, reactivating older faults. Excellent exposures near the village of Lemithou (Fig. 2) best illustrate the Kakopetria detachment and its polyphase deformational history. The detachment at Lemithou (Fig. 6a) separates structurally rotated dikes striking N60°W and dipping 28°NE from highly sheared isotropic gabbro. The fault itself is highly undulatory but generally dips ~40° NE. Assuming that the dikes were originally vertical and perpendicular to the detachment, they have been rotated (counterclockwise looking NW) approximately 75° with respect to the underlying gabbro. Restoration of dike magnetic vectors to the Troodos mean paleomagnetic vector (Moores & Vine 1971) about an approximately N12°W horizontal axis results in near-vertical, approximately N30°W-striking dike attitudes (S. Hurst personal communication 1988).

Major faults within the sheeted dike section (Fig. 6b) above the detachment at Lemithou generally strike N, dip E and have normal offset (Fig. 15a); the faults merge at depth with the detachment. In addition to the normal faults, several minor faults cutting the dike section have slickensides and offset senses incompatible with extensional deformation. Some of these have fault orientations similar to the normal faults but have low-raking slickensides indicating dextral movement (Fig. 15a).

Deformation of gabbro immediately beneath the detachment at Lemithou is much more complex than within the dike section. The gabbro is transected by a myriad of minor discrete brittle faults that serve to compartmentalize the unit into m- (Fig. 6a) to cm-size phacoids. The faults and phacoidal surfaces are slickensided and many are cross-cut at low angles by secondary striated fractures, interpreted in most cases to represent RM-type Riedel shears. In several places, the brittle faults cut an older fabric distinguished macroscopically by *S–C* structures and extensional shear bands (Fig. 6c). In thin section, this fabric is quite similar to mylonite fabrics found in ductile shear zones (Lister & Snoke 1984), but late laumontite alteration of plagioclase has masked any evidence for grain-scale plastic deformation.

Faults measured within the gabbro at Lemithou are shown stereographically on Fig. 15(b). While normal faults exist, most of the measurable fault population comprises E–W thrust and reverse faults and various strike-slip faults. All of the faults with reverse and thrust displacement are brittle features while the few apparently ductile fault zones mentioned above have normal displacement.

Faults measured elsewhere within deformed gabbro

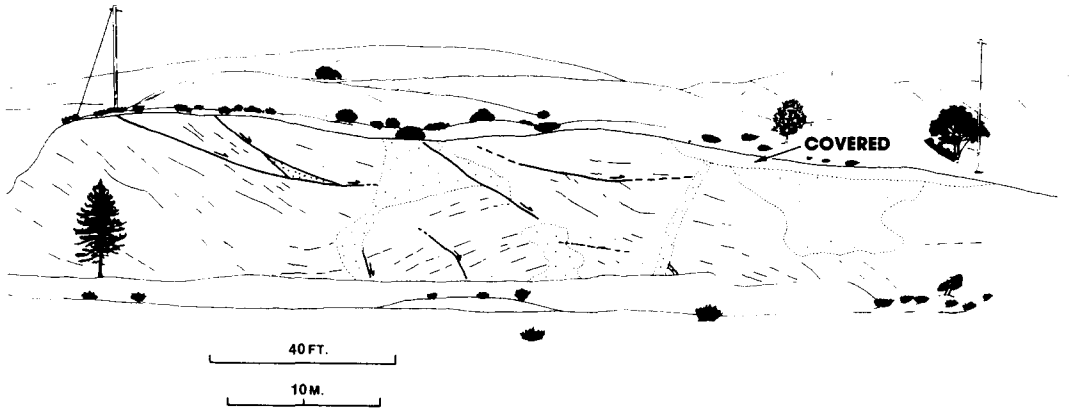

Fig. 10. Field sketch (direction of view is to the south) of roadcut exposures at locality 2 (Fig. 2). Light lines are traces of dike margins, bold lines are traces of normal faults, stippled areas are highly brecciated. Note antiformal outline of dikes within central part of outcrop.

of the Kakopetria detachment zone are shown in Fig. 16(a). The fault population is dominated by moderate-dipping faults which dip in the same direction as the faulted sheeted dike–gabbro contact and by high-angle, NE-striking faults. Sense of shear could be determined for very few of these faults. Many of the N-dipping faults have moderate- to low-raking slickensides. Others, however, have dip-slip slickensides for which thrust sense can be determined. Like the fault population at Lemithou, it is likely that the faults shown on Fig. 16(a) represent at least two periods of deformation; an earlier period related to extension and a later period related to compression. Relations shown on Fig. 5(a) illustrate the polyphase deformational history of the gabbro. In this area, numerous minor faults dip N at low to moderate angles. Many of these faults have low-raking slickensides but indeterminable offsets. A diabase dike, similar in composition to dikes of the sheeted complex, cut the faults and is little deformed. Minor thrust-sense offset of the dike occurs along several of the faults indicating reactivation of some of the surfaces following dike emplacement. These and similar relationships found elsewhere within gabbro immeditely beneath the Kakopetria detachment indicate a period of deformation close in age with ophiolite construction followed by a period of compressive deformation post-dating igneous activity.

Compressional structures

As discussed above, abundant minor faults within gabbro immediately beneath the Kakopetria detachment represent a post-extensional period of apparently compressive deformation. Structures observed within rocks of the Solea region above the Kakopetria detachment are dominantly extensional and related to graben formation. However, several faults cutting dikes and volcanics on both flanks of the graben are incompatible

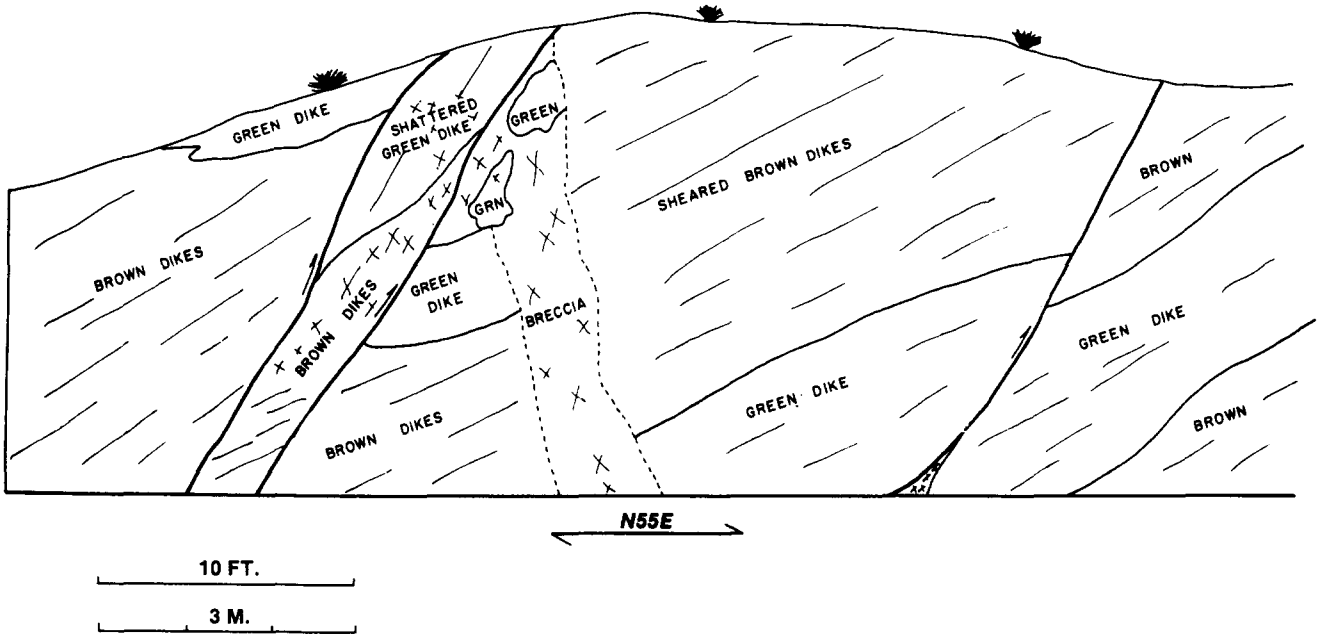

Fig. 11. Field sketch (direction of view is to the south) of exposures at locality 3 (Fig. 2). Light lines are traces of dike margins and bold lines are fault traces. Both dikes and faults with dip-slip slickensides strike N and dip E at this locality. Offsets of distinctive dike lithologies and RM-type Riedel shears on fault surfaces indicate reverse motion away from the axis of the Solea graben.

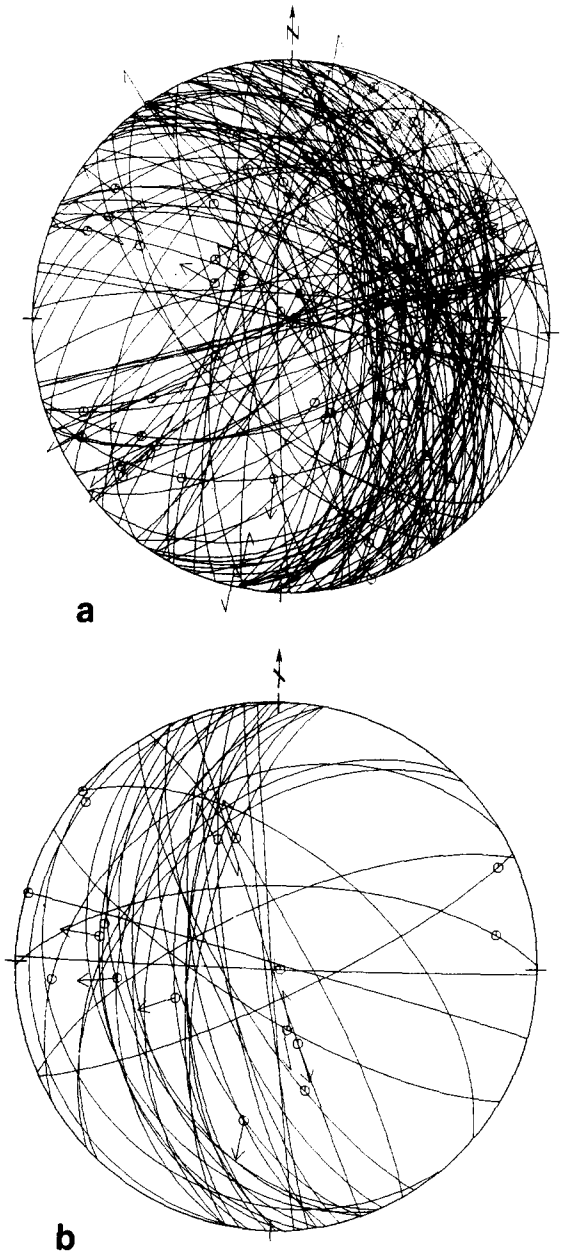

Fig. 12. Equal-area stereonets showing cyclographic traces of faults measured within sheeted dikes and volcanics of the western (a) and eastern (b) portions of the Solea graben. Symbols identical to those described in Fig. 9.

with the extensional structures and represent a later period of compressional deformation (Figs. 12a & b).

High-angle strike-slip faults occur in many areas of the graben. Some of these are undoubtedly related to extensional deformation, such as those shown on Fig. 9(a), as they are bounded by, and do not cross, low-angle normal faults and probably acted as small-scale transfer faults during hanging wall movement. Several others, however, are much larger-scale features and cross-cut extensional normal faults. In some areas, N-striking normal faults have been reactivated as strike-slip faults. Where cross-cutting slickensides are visible on such faults, low-raking slickensides overprint moderate- to high-raking slickensides (Fig. 6d).

Minor reverse and thrust faults also occur within the sheeted dike complex. In one area north of Moutoullas (Fig. 2, locality 5) dikes and normal faults dip NE at low angles (Fig. 17). Several of the faults in this area (Fig. 14) contain breccia which is preferentially altered to epidosite assemblages indicating their development early in the history of the graben (Bettison-Varga & Varga 1989). A late, vertical dike cross-cuts the rotated dikes. Several minor E–W-striking, N-dipping reverse faults cross-cut the dikes and several normal faults containing epidosite. Slickensides on the reverse faults are dip-slip and trend at high-angle to the trends of slickensides on normal faults. Reverse faulting is probably responsible for the synclinal curvature of dikes at this outcrop (Fig. 17).

The cross-cutting relations described above suggest a two-phase deformational history similar to that proposed for deformed gabbro in the vicinity of the Kakopetria detachment. Normal faults, some of which contain abundant sulfides and epidosite altered breccia (Bettison-Varga & Varga 1989), are related to extension and formation of the Solea graben. These early structures are cut by minor-displacement compressional structures that formed after hydrothermal alteration.

Kykko fault zone

A highly deformed region of diabase dikes runs for several kilometers in a nearly E–W direction west of Pedhoulas (Fig. 2, locality 4). Wilson (1959) named this zone the Kykko thrust and believed that deformation within this area was the result of N–S-directed compression. Detailed structural work in this area shows that deformational history is complex and polyphase.

Figure 18 shows deformational features in one area of the Kykko fault zone. Dikes are NE-striking within the fault zone and appear to be deflected to this attitude from more regional N–S trends (Wilson 1959). In contrast to the general relationship seen throughout the Solea graben, faults are often perpendicular to dike strikes. Minor dip-slip movement on closely spaced NW-striking NE-dipping faults has resulted in apparent folding of dikes when viewed parallel to dike strike (Fig. 18, bottom section). Many of the faults shown in Fig. 18 are normal faults and, viewed in a plane parallel to fault strike (Fig. 18, top section) high-angle faults are often bounded above and below by low-angle faults. Viewed perpendicular to fault strike (Fig. 18, bottom section) fault-bounded packages are wedge-shaped reflecting the probable spoon-shape of faults in three dimensions. Overall, the geometry of faults shown in this area is that of an extensional duplex.

In addition to normal faults, many minor reverse, thrust, and strike-slip faults exist within the Kykko fault zone, reflecting its polyphase history. All faults measured within the Kykko zone are shown stereographically in Fig. 16(b). Two dominant sets occur; NE-striking SE-dipping faults and NW-striking NE-dipping faults. Both sets have dominantly moderately to high-raking slickensides plunging ENE to ESE.

It is difficult to determine a chronology for faulting within the Kykko fault zone. Definitive cross-cutting

fault relations were not observed and both extensional and compressional faults appear to post-date hydrothermal alteration.

Paleostress analysis

Analysis of map patterns, the geometry of dike–fault relationships and interpretation of paleomagnetic data (Allerton & Vine 1987, Hurst *et al.* 1987) suggest that the NNW-trending Solea graben formed by structural rotation of fault blocks about a horizontal axis oriented more-or-less parallel to the graben axis. The stress conditions operative during graben subsidence cannot, however, be constrained by these data alone. Fault–slickenside data for faults related to formation of the Solea graben are analyzed below to solve for the orientations of principal stresses responsible for extension. Because the Solea graben was essentially *frozen* in place by spreading cessation (Varga & Moores 1985, in press), the stress orientations resulting from this analysis are those that existed at the Cretaceous seafloor spreading center.

Faults for which sense of shear could be determined in the field were analyzed using the iterative method described by Angelier (1984). This method solves for the best-fit stress tensor for a given fault/striae population by assuming that the slickenside orientation and sense of motion on individual faults have the same direction and sense, respectively, as the resolved shear stress on that surface. In this type of analysis, no assumptions are required for the original orientations of faults relative to stress axes; newly created faults and faults following preexisting anisotropies within the rock are taken into account within the solution. Results of the method are most accurate for fault systems with relatively small displacements. In practice, however, slickensides measured in the field commonly reflect only the latest increments of slip on fault surfaces so that the condition of small strain is often satisfied (Anderson & Barnhard 1986, J. Angelier written communication 1990). One test of this assumption is resolution of a stress tensor with either σ_1 or σ_3 in a subvertical orientation. Also, highly rotated fault systems (and, hence, rotated incremental strain axes) formed during protracted periods of deformation can often be recognized and accounted for because the axis of rotation is generally subparallel to a principal stress axis. For settings other than strike-slip settings, the horizontal axis of rotation will be σ_2, and σ_1 and σ_3 will lie within a vertical plane (see Angelier *et al.* 1981).

Separation of faults related to different deformational phases (i.e. extensional vs compressional) was guided by use of a phase separation program (J. Angelier personal communication 1985) based on algorithms described by Angelier & Manoussis (1980). The results of phase separation of a typical polyphase fault population is based solely on compatibility of individual faults with various hypothetical stress tensors. Although the results of this process on fault populations described in this paper mimic well the geologic relationships suggesting several fault generations, the separations cannot be considered rigorous as individual faults might be geometrically compatible with several phases. Excluded from the analyses are faults subsequently rotated such that their original shear sense is reversed (see Figs. 3 and 11).

Another problem encountered in analysis of fault populations using these techniques is in interpretation of high-angle, strike-slip faults. It is difficult to document whether such faults represent simple transfer, or accommodation, structures related to differential movement between extensional fault blocks or whether they represent periods of compressional deformation when the least principal stress direction (σ_3) was subhorizontal. Only in the latter case do the strike-slip faults constrain a relevant stress tensor. In the present study, faults interpreted as transfer faults within extensional fault blocks were not included in the analyses. These are faults that are bounded above and below by low-angle normal faults and whose strike is generally parallel to the trends of slickensides along local normal faults. Strike-slip faults are considered related to regional compression

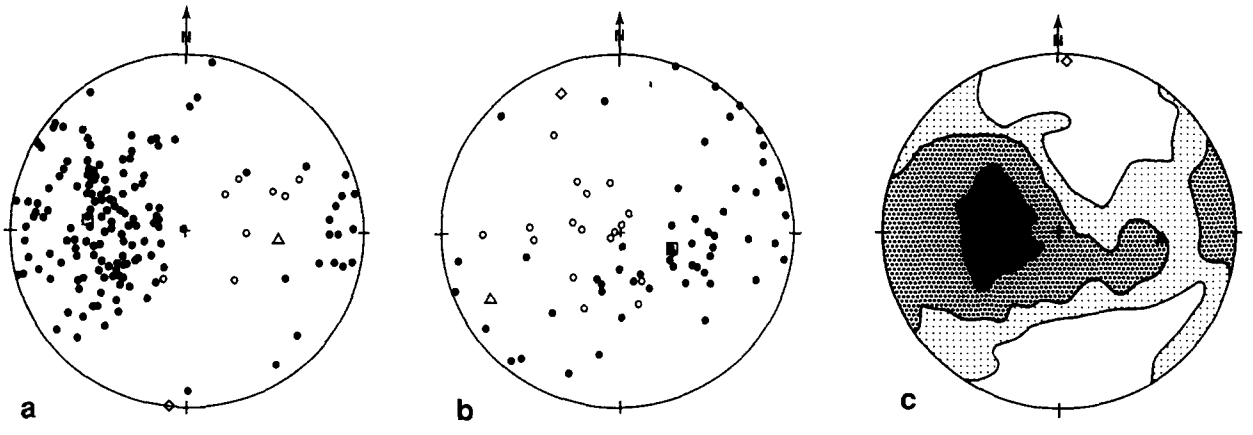

Fig. 13. Equal-area stereonets showing poles to dikes (filled circles) and volcanic bedding (open circles) in the western (a) and eastern (b) portions of the Solea graben. (c) Contour-density stereonet of combined data from both sides of the graben. Contours at 2, 4 and 10 times standard deviation from an assumed random distribution. In each diagram open square, triangle and diamond represent eigenvector orientations of greatest, intermediate, and smallest eigenvalues, respectively, for data distribution ellipsoid (Darot & Bouchez 1976).

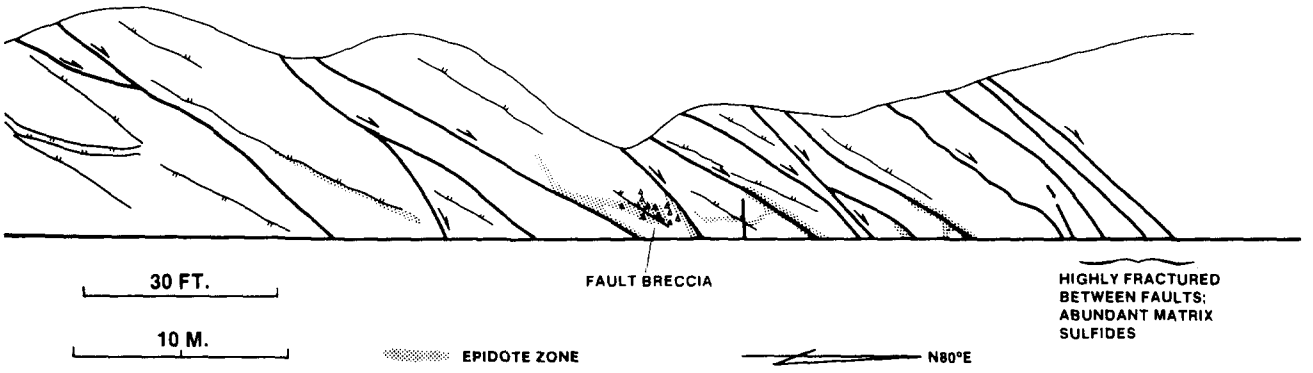

Fig. 14. Field sketch (direction of view is to the north) of the relationship between normal faults and areas of localized alteration where fractured diabase dikes have been converted to 'epidosite' mineral assemblages. Dark lines show normal faults and light lines with hachures show margins of highly rotated sheeted dikes. Outcrop is near location 5 and at the distal edge of the area of massive epidosite alteration (Fig. 2), after Bettison-Varga & Varga (1989).

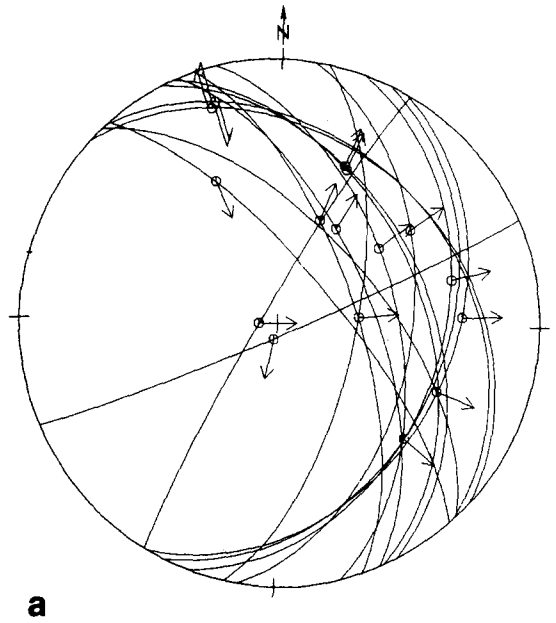

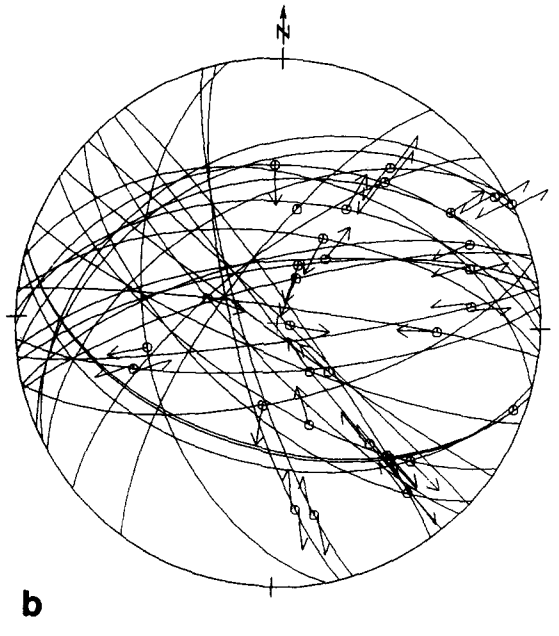

Fig. 15. Equal-area stereonets showing cyclographic fault traces and slip data for faults cutting (a) sheeted dikes and (b) gabbro at Lemithou.

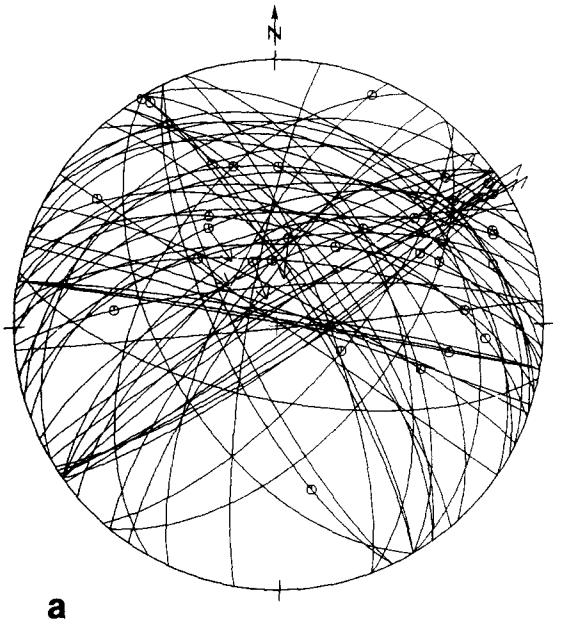

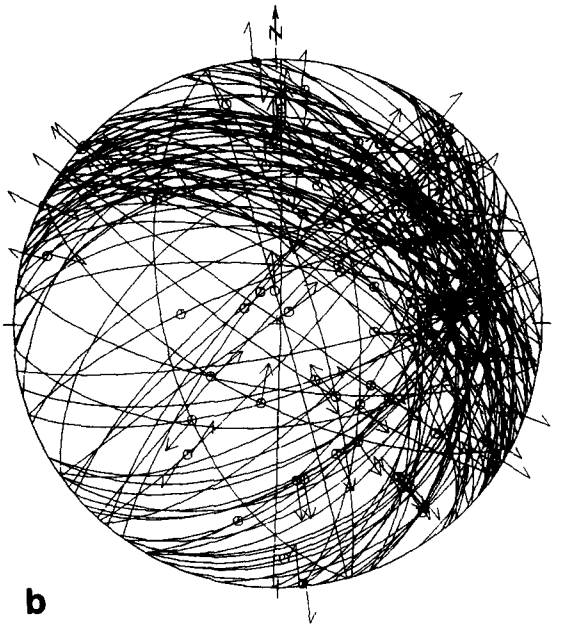

Fig. 16. Equal-area stereonets showing cyclographic fault traces and slip data for faults cutting (a) gabbro between Pedhoulas and Kakopetria and (b) sheeted dikes in the Kykko fault zone.

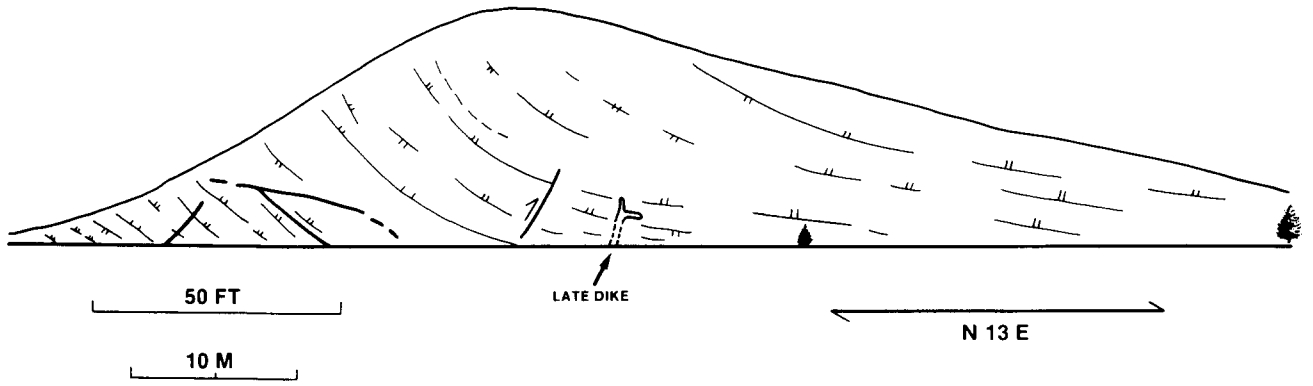

Fig. 17. Outcrop sketch (direction of view is to the east) of deformed dikes north of Moutoullas (locality 5, Fig. 2). Light lines with hachures are traces of dike margins and bold lines are fault traces. Dikes at south end of outcrop (to right) have attitudes typical of extensionally deformed dikes in this general area. In contrast, dikes at the north end of outcrop have been subsequently rotated and now define an open synform. This area also contains several N-dipping small reverse faults.

when either a consistent sense of shear exists for similarly striking faults or when a conjugate set of faults exists with opposite shear senses.

Fault populations analyzed include those measured in dikes and volcanics above the Kakopetria detachment, dikes and gabbro associated with the detachment exposures at Lemithou, gabbro beneath the detachment between Moutoullas and Kakopetria, and the Kykko fault zone. Results of phase separation and tensor analysis of faults in these areas are tabulated in Table 1. Given in Table 1 are the trend and plunge of the greatest (σ_1), intermediate (σ_2) and least (σ_3) principal stress directions, the stress ratio ($\Phi = (\sigma_2 - \sigma_3)/(\sigma_1 - \sigma_3)$), and the average angular error (T) between the calculated trac-

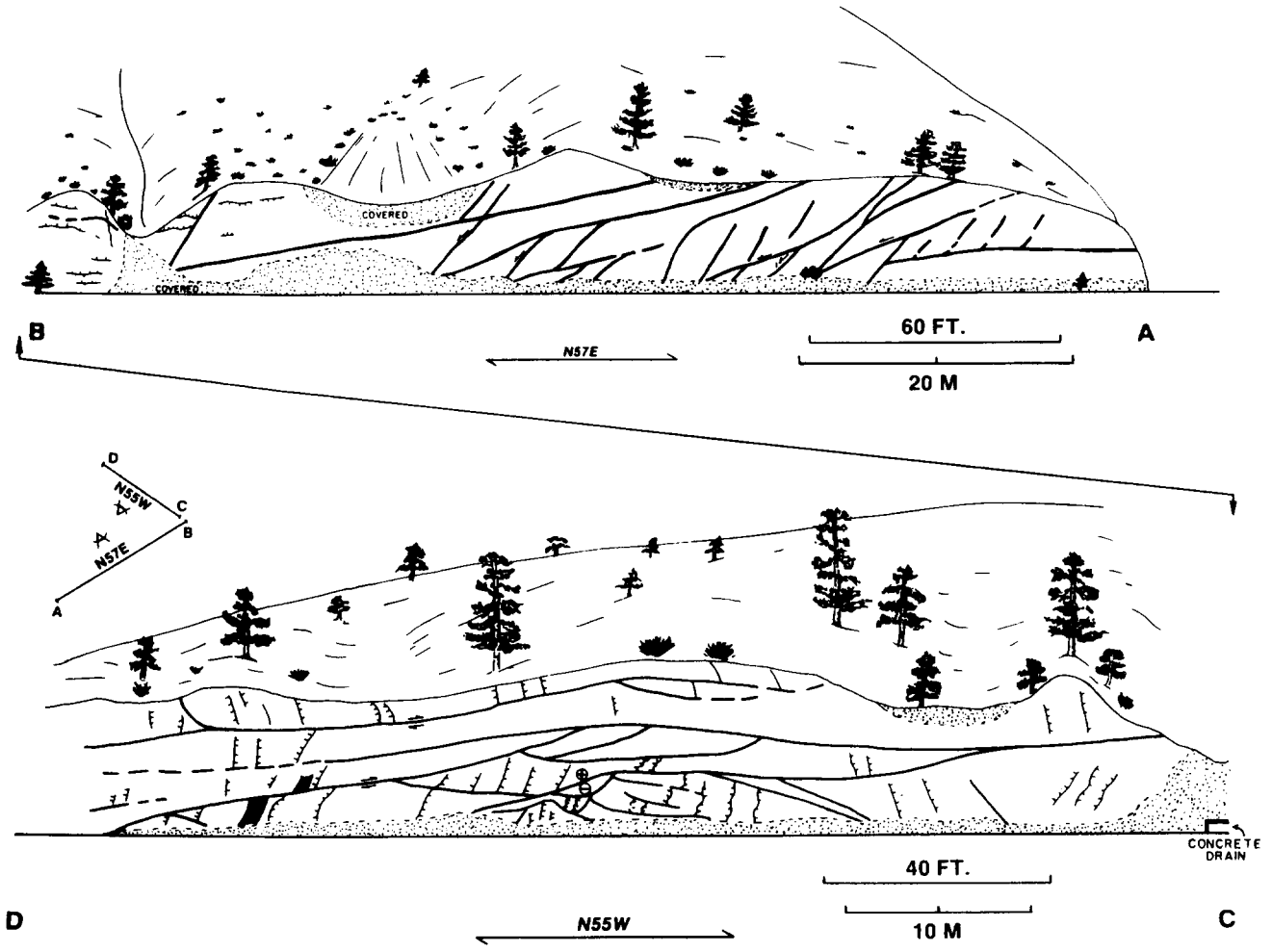

Fig. 18. Field sketches of deformed sheeted dikes within the Kykko fault zone. Inset drawing shows relative position of the two roadcuts and viewing direction. Top sketch is viewed essentially perpendicular to dike strike and parallel to fault (heavy lines) strikes. Note how faults link to form several extensional duplexes. Bottom sketch is viewed parallel to dike strike (thin lines, some with hatchures) and perpendicular to fault (heavy lines) stikes. Note lensoidal shape of fault-bounded packages. Slight non-parallelism between dike strikes and slip vectors of abundant microfaults has caused apparent folding of dikes in the central portion of bottom sketch.

Table 1. Fault and fault tensor data

Figure No.	n	σ_1	σ_2	σ_3	Φ	T
19(a)	25	024/82	198/08	288/01	0.18	12
19(b)	15	178/04	301/83	087/06	0.41	12
20(a)	16	024/83	143/03	233/06	0.24	13
20(b)	16	007/00	277/53	097/37	0.89	12
20(c)	9	189/15	282/09	042/72	0.99	12
20(d)	8	015/31	137/41	262/33	0.52	5
21(a)	37	349/76	157/14	247/03	0.36	14
21(b)	18	160/15	046/57	259/29	0.47	9

Φ = stress ratio: $(\sigma_2 - \sigma_3)/(\sigma_1 - \sigma_3)$.
T = average angle (in degrees) for fault population between calculated traction vector and slip line.

tion vector and the observed slip (slickenside) line (Angelier 1984).

Phase separation of 40 faults measured within dikes and volcanics in the western part of the Solea graben results in two stress tensors shown in Fig. 19(a). Faults compatible with the first tensor are largely NE- to NW-striking normal faults which dip E. Several NE-striking NW-dipping normal faults are also included. Faults included within this solution are compatible with WNW extension. The majority of strike-slip faults measured within the western Solea graben form a conjugate pair, with dextral faults oriented NW–SE and sinistral faults oriented NE–SW (Fig. 19b). These faults, and a single thrust fault are compatible with subhorizontal NNW compression and ENE extension.

Results of analysis of the combined fault population measured within gabbro and dike exposures associated with the Kakopetria detachment at Lemithou is shown in Fig. 20. Separation of the data into three stress tensors is necessary to utilize most of the available data. The first solution comprises normal faults which are collectively compatible with NE–SW extension. Two other tensors reflect subhorizontal NNE-oriented compression (Figs. 20b & c). The difference between these two 'compressional' solutions is that one contains dominantly strike-slip faults and is compatible with near-horizontal ESE-directed extension while the other contains reverse faults compatible with near-vertical extension. Because of the near-parallelism of σ_1 in these two tensors, they probably reflect different periods of the same general deformational event when σ_1 and σ_2 were reversed.

Faults measured within deformed gabbro beneath the Kakopetria detachment between Moutoullas and Kakopetria (Fig. 2) also reflect NNE-directed compression (Fig. 20d). However, the positions of σ_2 and σ_3 are unconstrained by this small fault sample. Both reverse and strike-slip faults are included in this solution and it is likely that they actually formed at different times during compression when σ_2 and σ_3 were reversed.

The complex of faults measured within the Kykko fault zone (Fig. 16b) are separable into two tensors. The first (Fig. 21a) reflects NE-directed extension and contains most of the normal faults observed within the zone. The second tensor (Fig. 21b) is compatible with NNW-directed compression and ENE extension. Many of the faults within this latter solution have orientations similar to normal faults shown in the extensional solution but have low-raking slickensides. Although cross-cutting slickensides were not observed on these faults, their orientation suggests that they were originally normal faults which were reactivated during regional compression.

The results of analysis of faults from various structural levels within the Solea graben are generally consistent from area to area. Most areas contain evidence for two deformational eposides; a SE–NW- to NE–SW-directed extensional event and a N–S-directed compressional event. Cross-cutting relationships demonstrate that the extensional event occurred early in the formation of the graben, at or near an oceanic spreading center, in close association with large-scale hydrothermal events and late intrusive activity. In contrast, the compressional event post-dates any recognizable hydrothermal or igneous events related to seafloor spreading and prob-

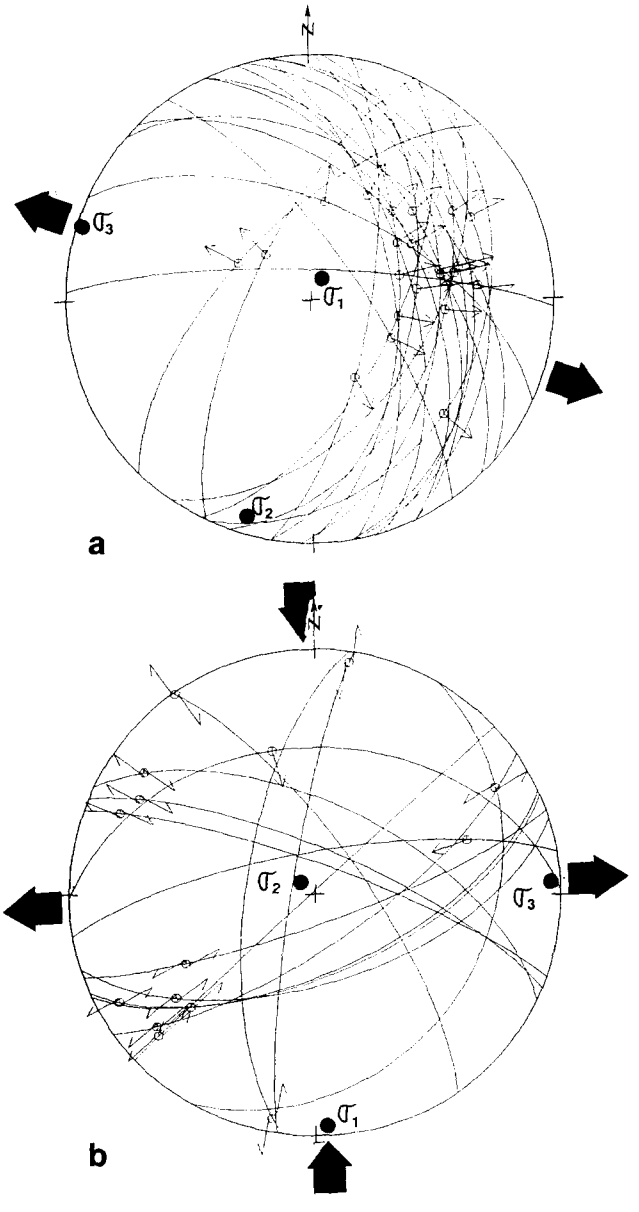

Fig. 19. Equal-area stereonets showing phase separation of faults cutting dikes in the western part of the Solea graben (Fig. 12a). σ_1, σ_2, σ_3 represent orientations of greatest, intermediate and least principal stresses, respectively, compatible with faults in each diagram.

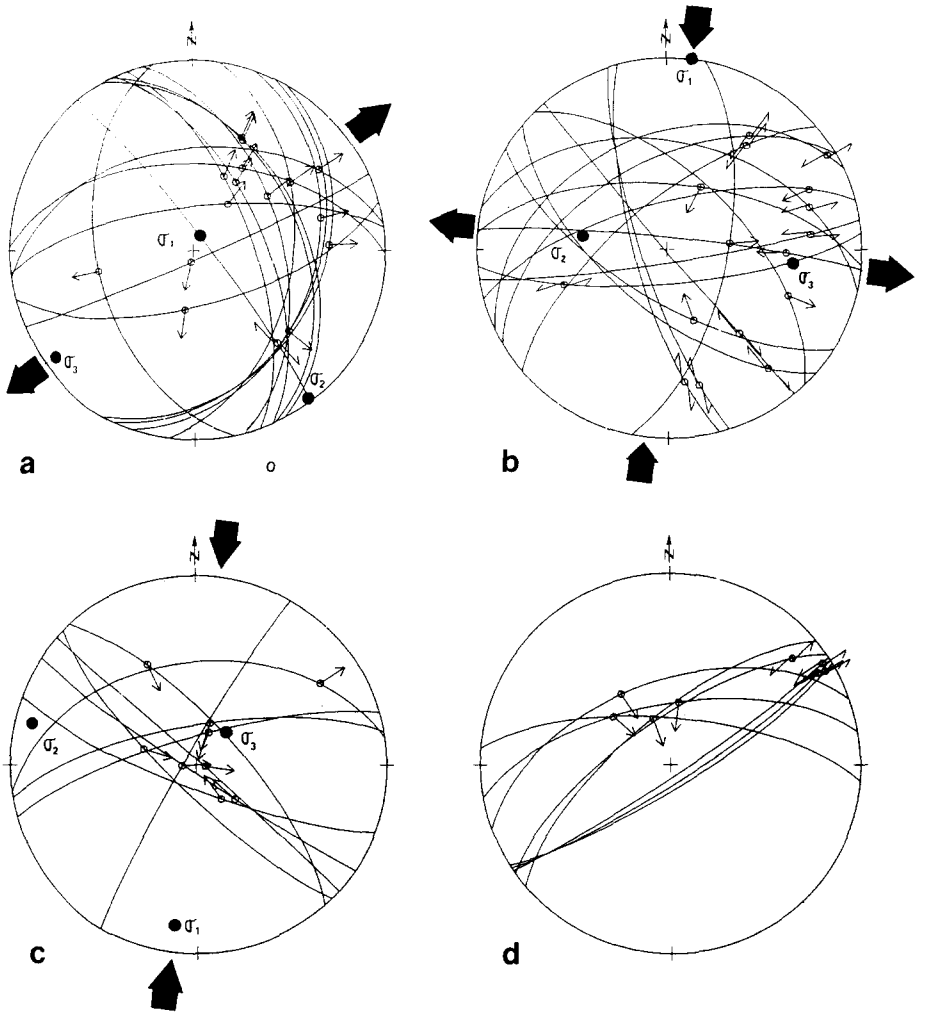

Fig. 20. Equal-area stereonets showing phase separation of faults cutting (a–c) dikes and gabbros associated with the Kakopetria detachment at Lemithou (Fig. 15) and (d) gabbro between Pedhoulas and Kakopetria (Fig. 16a). Symbols as in Fig. 19.

ably reflects minor deformation during latest-Cretaceous to Recent obduction and uplift of the ophiolite (Robertson & Woodcock 1980).

CONCLUSIONS AND SIGNIFICANCE TO OCEAN RIDGE PROCESSES

The formation of the Solea structural graben appears to have resulted during a brief period of tectonic extension at a spreading center when magma supply was insufficient to keep pace with plate separation (Varga & Moores 1986, in press). The dimensions of the Solea graben are similar to those of axial grabens formed along magma-starved portions of slow-spreading ridges (Varga & Moores in press) where extensive deformation occurs during periods of amagmatic tectonic extension (Macdonald 1982, Karson *et al.* 1987, Karson in press). Within the upper crustal section of the Solea graben, tectonic extension was accommodated by thinning through slip on normal faults that dip toward a common axis of symmetry. Individual normal faults are dominantly planar in cross-section, but link at the outcrop scale to form approximately listric geometries. Exposures of normal faults parallel to slip direction suggest that they have gentle concave-upward spoon shapes. Kinematic structures preserved along and near fault surfaces indicate these faults are the result of brittle deformation.

Mean dike dips for the central portions of the Solea graben (Fig. 13c) indicate that dikes have been rotated 40–50° on average. Rotations of this magnitude are in accord with interpretation of rotations of oceanic rocks based on magnetic inclination anomalies (Verosub & Moores 1981) and with rare, direct observation of tilted volcanics and dikes on the seafloor (Karson 1987). However, in several areas of the graben, dikes have been rotated to very low angles. Repeated normal faulting has resulted in >90° rotation of some dikes. In addition, rotation of some antithetic normal faults during extension caused reversal in offset sense. At modern ridges, apparent reverse faults produced in this manner should have strike directions parallel to strikes of other normal faults and hanging wall motions *away* from graben axes.

During tectonic extension in the Solea graben, σ_3 was

oriented more-or-less perpendicular to the physiographic axis of the graben, to the axis of structural rotation, and to the pre-rotational orientation of dikes in the sheeted complex. Assuming that dikes of upper oceanic crust are intruded approximately parallel to the σ_1/σ_2 plane (Karson 1987), stress orientations for magmatically compensated plate separation were subparallel to those operating during tectonic extension. This result is similar to that from paleostress analysis of rift-related, neotectonic normal faults on Iceland (Bergerat *et al.* 1990). Fault data from the Solea graben do not define a period of rift-perpendicular compression as is observed in regions of Iceland (Bergerat *et al.* 1990) and in *in situ* stress measurements of some young oceanic crust (Moos & Zoback 1989).

Normal faults within upper crustal units of the Solea graben appear to merge into a low-angle normal fault at the sheeted dike–plutonic complex contact. Rare, relict *S–C* fabrics within gabbro immediately below the fault suggest that early deformation related to detachment formation may have been partially ductile. It is important to emphasize that the detachment zone between dikes and plutonic rocks is best developed in those areas of the Troodos ophiolite where extension within the upper crustal section is the greatest, as indirectly evidenced by degree of apparent structural rotations. In some areas where dikes retain their original steep attitudes, the contact between dikes and gabbros appears little deformed (Varga & Moores in press).

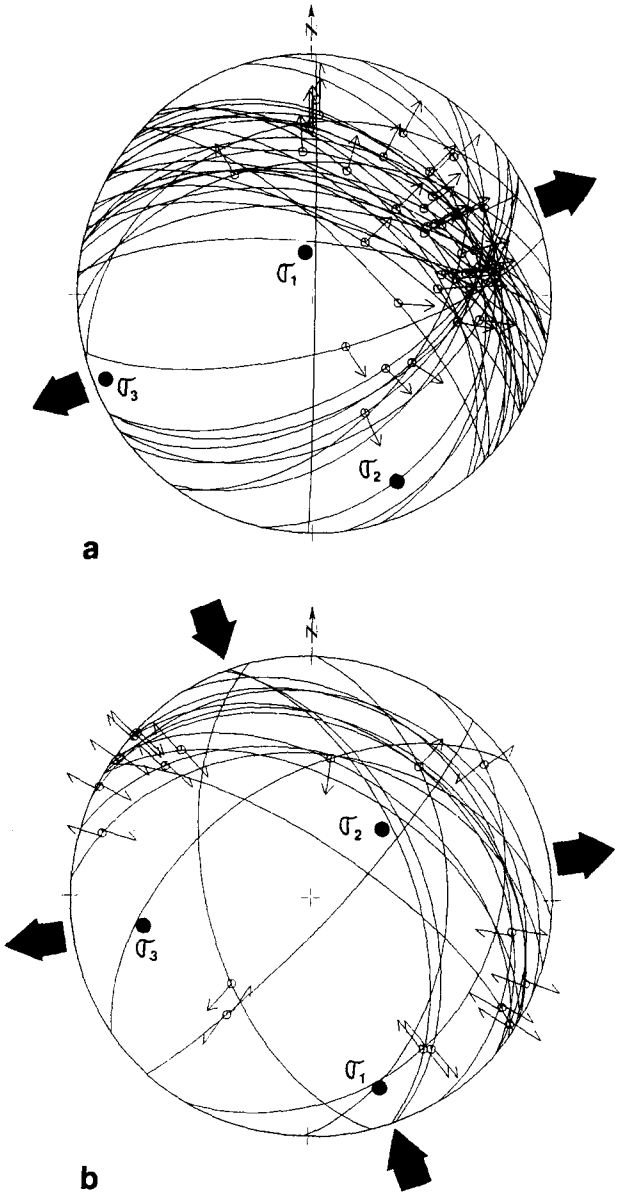

Fig. 21. Equal-area stereonets showing phase separation of faults cutting sheeted dikes within the Kykko fault zone (Fig. 16b). Symbols as in Fig. 19.

The documented link between extensional normal faulting of upper crustal rocks in the Solea graben with a basal detachment zone supports detachment models postulated for some magma-starved segments of the Mid-Atlantic Ridge. In the MARK (Mid-Atlantic Ridge at the Kane fracture zone) area, deformed and metamorphosed plutonic rocks (Karson & Dick 1984) and serpentinites (Leg 109 Scientific Drilling Party 1986) have been exposed by faulting. Karson *et al.* (1987) and Karson (in press) postulate that these deformed lower crustal and upper mantle rocks lie in the footwall of a master extensional detachment fault dipping shallowly beneath the spreading center and penetrating the Moho. The position of the Kakopetria detachment at the dike–gabbro contact contrasts to observations for detachment within the peridotite section of the Josephine ophiolite (Norrell *et al.* 1989) and at the crust–mantle transition of the Bay of Islands ophiolite (Casey 1987). This difference may reflect the relative lack of peridotite exposures within the Troodos complex. Lying at a constant lithologic horizon (sheeted dike–plutonic contact), the Kakopetria detachment appears to have been originally approximately horizontal, at least across its current area of exposure. However, the detachment may dip to the east beneath the graben axis and ramp down to deeper levels beyond the present plutonic–mantle exposures of Mt Olympos (Fig. 1).

Late diabase dikes and high-level gabbro stocks cut both the detachment, rotated upper plate rocks and associated normal faults, demonstrating that the Solea graben formed in a near-axial position relative to an oceanic spreading center. Emplacement of these magmas into greatly thinned and deformed crust drove a large-scale sea water-dominated hydrothermal system in the western part of the graben that resulted in formation of black smoker-type ore bodies within the volcanic section of the graben (Schiffman *et al.* 1987). Hydrothermal fluids in the upflow zone, now characterized by presence of epidosites (Fig. 2), rose along the interlocking network of graben-related normal faults (Bettison-Varga & Varga 1989). This sequence is analogous to that postulated for the neovolcanic zone in the MARK area. There, intrusion of high-level magmas into the crust and establishment of a vigorous hydrothermal system followed detachment faulting and extreme lithospheric thinning (Karson in press).

Prior to final cessation of magmatic activity in the Solea graben, the detachment fault was segmented along several N-trending high-angle normal faults (Fig. 2). Emplacement of plagiogranite along the presumed

trace of one of these fault zones (between Lemithou and Moutoullas; Fig. 2) and presence of gossan along the north trace of the fault running southeast from near the Apliki mine (Fig. 2) (S. Hurst personal communication 1987), indicates that these structures also formed at, or near, a former spreading center. Documented offset along one of these is on the order of 300–800 m (S. Hurst personal communication 1987), similar in dimension to faults defining some median valleys of the Mid-Atlantic Ridge (Macdonald 1982).

Cessation of spreading in the Solea area preserved the physiographic graben and its underlying mantle diapir (Varga & Moores in press). Subsequent Plio-Pleistocene exposure of the ophiolite is probably due, in part, to gentle arching of the entire complex about an WNW-trend and to enhanced uplift of the central Troodos due to partial serpentinization of the mantle section (Gass & Masson-Smith 1963, Robertson & Woodcock 1980). Minor, post-magmatic faults measured within the Solea graben formed during N–S compression, probably during arching and obduction of the ophiolite. In the Solea area, much of this deformation was focused along several pre-existing, low-angle fault zones including the Kakopetria detachment and the Kykko fault zone. Tensor analysis of these fault data are consistent with earthquake focal mechanisms indicating thrusting on a N-dipping zone beneath Cyprus (Rotstein & Kafka 1982) and with other geologic and gravity data indicating N–S compression during obduction (Robertson & Woodcock 1980, Lapierre *et al.* 1988).

Acknowledgements—I thank Eldridge Moores, Steve Hurst, Peter Schiffman, Lori Bettison-Varga and Brian Smith for their input and help during field work and formulation of ideas presented in this paper. I am also grateful for the hospitality of Jacques Angelier and for use of his computer routines for stress tensor reduction of fault data. Presentation of these ideas was greatly improved by the detailed and knowledgeable reviews of Jeff Karson and Simon Allerton. This research was supported by NSF grants EAR-830695 and EAR-8610503 to Eldridge Moores and Peter Schiffman and by Unocal Science and Technology Division.

REFERENCES

Allerton, S. & Vine, F. J. 1987. Spreading structure of the Troodos ophiolite, Cyprus: Some paleomagnetic constraints. *Geology* **15**, 593–597.

Anderson, R. E. & Barnhard, T. P. 1986. Genetic relationship between faults and folds and deterionation of Laramide and neotectonic paleostress, western Colorado Plateau–Transition Zone, central Utah. *Tectonophysics* **5**, 335–357.

Anderson, R. N., Honnorez, J., Becker, K., Adamson, A. Alt, J., Emmermann, R., Kempton, P., Kinoshita, H., Lavern, C., Mottl, M. & Newmark, R. 1982. DSDP Hole 504B, the first reference section over 1 km through Layer 2 of the oceanic crust. *Nature* **300**, 589–594.

Angelier, J. 1984. Tectonic analysis of fault slip data sets. *J. geophys. Res.* **89**, 5835–5848.

Angelier, J., Colletta, B., Chorowicz, J., Ortlieb, L. & Rangin, C. 1981. Fault tectonics of the Baja California peninsula and the opening of the Sea of Cortez, Mexico. *J. Struct. Geol.* **3**, 347–357.

Angelier, J. & Manoussis, S. 1980. Classification automatique et distinction des phases superposees en tectonique de failles. *C. r. Acad. Sci., Paris* **D290**, 651–664.

Axen, G. J. 1988. The geometry of planar domino-style normal faults above a dipping basal detachment. *J. Struct. Geol.* **10**, 405–411.

Ballard, R. D. & Van Andel, T. H. 1977. Morphology and tectonics of the inner rift valley at lat 36°50′N on the Mid-Atlantic Ridge. *Bull. geol. Soc. Am* **88**, 507–530.

Bergerat, F., Angelier, J. & Villemin, T. 1990. Fault systems and stress patterns on emerged oceanic ridge: a case study in Iceland. *Tectonophysics* **179**, 183–197.

Bettison-Varga, Lori & Varga, R. J. 1989. Timing of extension, late-stage intrusive activity, hydrothermal upwelling and ore formation, Solea axial valley, Troodos ophiolite, Cyprus. *EOS* **70**, 1399.

Casey, J. F. 1987. Strain localization within oceanic lithosphere at mid-ocean ridges: Implications for the depths of sea water penetration. *EOS* **68**, 1509.

Chester, F. M., Friedman, M. & Logan, J. M. 1985. Foliated fault gouge. *Tectonophysics* **111**, 139–146.

Constantinou, G. & Grovett, G. J. S. 1973. Geology, geochemistry and genesis of Cyprus sulphide deposits. *Econ. Geol.* **68**, 843–858.

Darot, M. & Bouchez, J.-L. 1976. Study of directional data distributions from principal preferred orientation axes. *J. Geol.* **84**, 239–247.

Fox, P. J., Detrick, R. S. & Purdy, G. M. 1980. Evidence for crustal thinning near fracture zones: Implications for ophiolites. In: *Ophiolites, Proceedings of the International Ophiolite Symposium, Cyprus*, 1979 (edited by Panayiotou, A.). Cyprus Geol. Surv. Dept, Nicosia, 161–168.

Gallo, D. G. & Tamayo Tectonic Team. 1984. Tectonics at the intersection of the east Pacific Rise with Tamayo transform fault. *Mar. geophys. Res.* **6**, 159–185.

Gass, I. G. & Masson-Smith, D. 1963. The geology and gravity anomalies of the Troodos massif, Cyprus. *Phil. Trans. R. Soc, Lond.* **A255**, 417–467.

Gibbs, A. D. 1983. Balanced cross-section constructions from seismic sections in areas of extensional tectonics. *J. Struct. Geol.* **5**, 152–160.

Gibbs, A. D. 1984. Structural evolution of extensional basin margins. *J. geol. Soc. Lond.* **141**, 609–620.

Harper, G. D. 1982. Evidence for large-scale rotations at spreading centers from the Josephine ophiolite. *Tectonophysics* **82**, 25–44.

Harrison, C. G. A. & Stieltjes, L. 1977. Faulting within the median valley. *Tectonophysics* **38**, 137–144.

Hurst, S. D., Moores, E. M. & Varga, R. J. 1987. Structure of the Solea graben, Cyprus from gravity and paleomagnetic investigations. *Geol. Soc. Am. Abs. w. Prog.* **19**, 390.

Jackson, J. & McKenzie, D. 1983. The geometrical evolution of normal fault systems. *J. Struct. Geol.* **5**, 471–482.

Karson, J. A. 1982. Reconstructed seismic velocity structure of the Lewis Hills massif and implications for oceanic fracture zones. *J. geophys. Res.* **87**, 961–978.

Karson, J. A. 1987. Factors controlling the orientation of dykes in ophiolites and oceanic crust. In: *Mafic Dyke Swarms* (edited by Halls, H. C. & Fahring, W. F.). *Spec. Pap. geol. Soc. Can.* **34**, 229–241.

Karson, J. A. In press. Seafloor spreading on the Mid-Atlantic ridge: Implications for the structure of ophiolites and oceanic lithospheres produced in slow-spreading environments. In: *Proceedings Troodos '87, Ophiolites and Oceanic Crust* (edited by Moores, E. M., Panayiotou, A., Malpas, J. G. & Xenophontos, C.). Cyprus Geol. Surv. Dept, Nicosia.

Karson, J. A. & Dick, H. J. B. 1983. Tectonics of ridge-transform intersections at the Kane fracture zone. *Mar. geophys. Res.* **6**, 51–98.

Karson, J. A. & Dick, H. J. B. 1984. Deformed and metamorphosed oceanic crust on the mid-Atlantic ridge. *Ofioliti* **9**, 279–302.

Karson, J. A. & Oceanographer Tectonic Research Team. 1984. The geology of the Oceanographer transform: the ridge-transform domain. *Mar. geophys. Res.* **6**, 109–141.

Karson, J. A., Thompson, G., Humphris, S. E., *et al.* 1987. Along-axis variations in seafloor spreding in the MARK area. *Nature* **328**, 681–685.

Karson, J. A. & Winters, A. T. 1987. Tectonic extension on the Mid-Atlantic ridge. *EOS* **68**, 1508.

Lapierre, H., Angelier, J., Cogne, X., Grand, T. & Mascle, G. 1988. Tectonique superposee de la zone de faille d'Arakapas (Massif de Troodos, Chypre). *Geodinamica Acta* **2**, 197–206.

Leg 109 Shipboard Scientific Party. 1986. Coring the crust and mantle. *Nature* **323**, 492–493.

Leg 118 Shipboard Scientific Party. 1988. Plutonic rocks in fracture zones. *Nature* **333**, 115–116.

Lister, G. S. & Snoke, A. W. 1984. S–C mylonites. *J. Struct. Geol.* **6**, 283–297.

Macdonald, K. C. 1982. Mid-oceanic ridges: Fine scale tectonic,

volcanic and hydrothermal processes within the plate boundary zone. *Annu. Rev. Earth & Planet. Sci.* **10**, 155–190.

Macdonald, K. C. 1986. The crest of the Mid-Atlantic Ridge. In: *Geology of North America Volume* M: *The Western North Atlantic Region* (edited by Vogt, P. R. & Tucholke, B. E.). Geol. Soc. Am., 51–68.

Macdonald, K. C. & Atwater, T. M. 1978. Evolution of rifted ocean ridges. *Earth Planet. Sci. Lett.* **39**, 319–327.

McClain, J. S., Orcutt, J. A. & Burnett, M. 1985. The East Pacific Rise in cross section: A seismic model. *J. geophys. Res.* **90**, 8627–8639.

Miller, E. L., Gans, P. B. & Garing, J. 1983. The Snake Range decollement: An exhumed mid-Tertiary ductile–brittle transition. *Tectonics* **2**, 239–263.

Moores, E. M. 1982. Origin and emplacement of ophiolites. *Rev. Geophys. & Space Phys.* **20**, 735–760.

Moores, E. M. & Jackson, E. D. 1974. Ophiolites and oceanic crust. *Nature* **250**, 136–139.

Moores, E. M., Robinson, P. T., Malpas, J. & Xenophontos, C. 1984. Model for the origin of the Troodos massif, Cyprus and other Mideast ophiolites. *Geology* **12**, 500–503.

Moores, E. M., Varga, R. J., Verosub, K. L. & Ramsden, T. W. In press. Regional structure of the Troodos dike complex. In: *Proceedings Troodos '87, Ophiolites and Oceanic Crust* (edited by Moores, E. M., Panayiotou, A., Malpas, J. G. & Xenophontos, C.). Cyprus Geol. Surv. Dept, Nicosia.

Moores, E. M. & Vine, F. J. 1971. Troodos Massif, Cyprus and other ophiolites as oceanic crust: evaluation and implications. *Phil. Trans. R. Soc. Lond.* **A268**, 443–466.

Moos, D. & Zoback, M. D. 1989. Determination of in situ stress orientation and magnitude from observations of wellbore failure. EOS **70**, 1301.

Mutter, J. C. & North Atlantic Transect (NAT) Study Group. 1985. Multichannel seismic images of the oceanic crust's internal structure: Evidence for a magma chamber beneath the Mesozoic Mid-Atlantic Ridge. *Geology* **13**, 629–632.

Miyashiro, A. 1973. The Troodos ophiolite was probably formed in an island arc. *Earth Planet. Sci. Lett.* **19**, 218–224.

Nicolas, A., Ceuleneer, G., Boudier, F. & Misseri, M. 1988. A structural mapping in the Oman ophiolites: mantle diapirism along an oceanic ridge. *Tectonophysics* **151**, 27–57.

Norrell, G. T. & Harper, G. D. 1988. Detachment faulting and amagmatic extension at mid-ocean ridges: The Josephine ophiolite as an example. *Geology* **16**, 827–830.

Norrell, G. T., Teixell, A. & Harper, G. D. 1989. Microstructure of serpentinite mylonites from the Josephine ophiolite and serpentinization in retrogressive shear zones, California. *Bull. geol. Soc. Am.* **101**, 673–682.

Nur, A., Hagai, R. & Scotti, O. 1986. Fault mechanics and the kinematics of block rotations. *Geology* **14**, 746–749.

Pallister, J. S. 1981. Structure of the sheeted dike complex of the Semail ophiolite near Ibra, Oman. *J. geophys. Res.* **86**, 2661–2672.

Pearce, J. A. & Cann, J. R. 1973. Tectonic setting of basic volcanic rocks determined using trace element analyses. *Earth Planet. Sci. Lett.* **19**, 290–300.

Petit, J. P. 1987. Criteria for the sense of movement on fault surfaces in brittle rocks. *J. Struct. Geol.* **9**, 597–608.

Ramsden, T. W. 1987. The Structural Geology and Paleomagnetism of the Sheeted Dike Complex in the Mitsero-Arakapas area, Troodos Ophiolite, Cyprus. Unpublished M.S. thesis. University of California, Davis.

Rautenschlein, M., Jenner, G. A., Hertogen, J., Hoffman, R. Schmincke, H.-U. & White, W. M. 1985. Isotopic and trace element compositions of volcanic glasses from the Akaki canyon, Cyprus: Implications for the origin of the Troodos ophiolite. *Earth Planet. Sci. Lett.* **75**, 369–383.

Robertson, A. H. F. & Woodcock, J. F. 1980. Tectonic setting of the Troodos massif in the east Mediterranean. In: *Ophiolites, Proceedings of the International Ophiolite Symposium, Cyprus*, 1979 (edited by Panayiotou, A.). Cyprus Geol. Surv. Depart, Nicosia, 36–49.

Rotstein, Y. & Kafka, A. L. 1982. Seismotectonics of the southern boundary of Anatolia, eastern Mediterranean region: subduction, collision and arc jumping. *J. geophys. Res.* **87**, 7694–7706.

Schiffman, P., Bettison, L. A. & Smith, B. M. In press. Mineralogy and geochemistry of epidosites from the Solea graben, Troodos ophiolite, Cyprus. In: *Proceedings Troodos '87, Ophiolites and Oceanic Crust* (edited by Moores, E. M., Panayiotou, A., Malpas, J. G. & Xenophontos, C.). Cyprus Geol. Surv. Dept, Nicosia.

Schiffman, P. & Smith, B. M. 1988. Petrology and oxygen isotope geochemistry of a fossil seawater hydrothermal system within the Solea graben, northern Troodos ophiolite, Cyprus. *J. geophys. Res.* **93**, 4612–4624.

Schiffman, P., Smith, B. M., Varga, R. J. & Moores, B. M. 1987. Geometry, conditions, and timing of off-axis hydrothermal metamorphism and ore-deposition in the Solea graben. *Nature* **235**, 423–425.

Sleep, J. H. & Rosendahl, B. R. 1979. Topography and tectonics of mid-ocean ridge axes. *J. geophys. Res.* **84**, 6831–6839.

Tapponnier, P. & Francheteau, J. 1978. Necking of the lithosphere and the mechanics of slowly accreting plate boundaries. *J. geophys. Res.* **83**, 3955–3970.

Varga, R. J. & Moores, E. M. 1985. Spreading structure of the Troodos ophiolite. *Geology* **13**, 846–850.

Varga, R. J. & Moores, E. M. 1986. Episodic tectonic vs. steady state magmatic spreading in oceanic crust: Evidence from the Troodos ophiolite. *Geol. Soc. Am. Abs. w. Prog.* **18**, 194.

Varga, R. J. & Moores, E. M. In press. Intermittent magmatic spreading and tectonic extension in the Troodos ophiolite: Implications for exploration for black smoker-type ore deposits. In: *Proceedings Troodos '87, Ophiolites and Oceanic Crust* (edited by Moores, E. M., Panayiotou, A., Malpas, J. G. & Xenophontos, C.). Cyprus Geol. Surv. Dept, Nicosia.

Verosub, K. L. & Moores, E. M. 1981. Tectonic rotations in extensional regimes and their paleomagnetic consequences for oceanic basalts. *J. geophys. Res.* **86**, 6335–6349.

Vogt, P. R. & Tucholke, B. E. 1986. Imaging the ocean floor: History and state of the art. In: *Geology of North America Volume* M: *The Western North Atlantic Region* (edited by Vogt, P. R. & Tucholke, B. E.). Geol. Soc. Am., 19–44.

Wernicke, B. P. 1985. Uniform sense of normal simple shear of the continental lithosphere. *Can. J. Earth Sci.* **22**, 108–125.

Wernicke, B. P. & Burchfiel, B. C. 1982. Modes of extensional tectonics. *J. Struct. Geol.* **4**, 105–115.

White, R. S. 1984. Atlantic oceanic crust: Seismic structure of a slow-spreading ridge. In: *Ophiolites and Oceanic Crust* (edited by Gass, I. G., Lippard, S. J. & Shelton, A. W.). *Spec. Publs geol. Soc. London.* **13**, 101–111.

Williams, G. & Vann, I. 1987. The geometry of listric normal faults and deformation in their hangingwalls. *J. Struct. Geol.* **9**, 789–795.

Wilson, R. A. M. 1959. The Geology of the Xeros–Troodos Area. *Mem. Cyprus Geol. Surv. Dept* **1**.